

The Optical/Near-IR Colours of Red Quasars

Paul J Francis ^{1,2} Matthew T. Whiting ³ Rachel L. Webster ³

¹ Research School of Astronomy and Astrophysics, Australian National University, Canberra
ACT 0200
pfrancis@mso.anu.edu.au

² Joint appointment with the Department of Physics and Theoretical Physics, Faculty of Science

³ School of Physics, University of Melbourne, Parkville, VIC 3052
mwhiting,rwebster@physics.unimelb.edu.au

Abstract

We present quasi-simultaneous multi-colour optical/near-IR photometry for 157 radio selected quasars, forming an unbiassed sub-sample of the Parkes Flat-Spectrum Sample. Data are also presented for 12 optically selected QSOs, drawn from the Large Bright QSO Survey.

The spectral energy distributions of the radio- and optically-selected sources are quite different. The optically selected QSOs are all very similar: they have blue spectral energy distributions curving downwards at shorter wavelengths. Roughly 90% of the radio-selected quasars have roughly power-law spectral energy distributions, with slopes ranging from $F_\nu \propto \nu^0$ to $F_\nu \propto \nu^{-2}$. The remaining 10% have spectral energy distributions showing sharp peaks: these are radio galaxies and highly reddened quasars.

Four radio sources were not detected down to magnitude limits of $H \sim 19.6$. These are probably high redshift ($z > 3$) galaxies or quasars.

We show that the colours of our red quasars lie close to the stellar locus in the optical: they will be hard to identify in surveys such as the Sloan Digital Sky Survey. If near-IR photometry is added, however, the red power-law sources can be clearly separated from the stellar locus: IR surveys such as 2MASS should be capable of finding these sources on the basis of their excess flux in the K -band.

Keywords: Quasars: general - Methods: observational

1 INTRODUCTION

It was long believed that quasars are blue. The optical/near-IR colours of optically selected QSOs are indeed uniformly very blue (eg. Neugebauer et al. 1987, Francis 1996). It was therefore a surprise when substantial numbers of extremely red quasars were identified in radio-selected samples (eg. Rieke, Lebofsky & Wisniewski 1982, Ledden & O'Dell 1983, Webster et al. 1995, Stickel, Rieke, Kühr 1996). The biggest sample of these objects is that of Webster et al, who were studying a sample of radio-loud quasars with flat radio spectra: the Parkes Half-Jansky Flat-Spectrum survey, a complete sample of 323 sources with fluxes at 2.7 GHz ($S_{2.7}$) of greater than 0.5 Jy, and radio spectral indices α ($S_\nu \propto \nu^\alpha$) with $\alpha > -0.5$ as measured between 2.7 and

5.0 GHz (Drinkwater et al. 1997). While some of these Parkes sources had $B_J - K_n$ colours as blue as any optically selected QSOs, most had redder $B_J - K_n$ colours, and some were amongst the reddest objects on the sky.

Why should the Parkes sources be so red? A variety of theories were proposed:

- The B_J magnitudes of the Parkes sample were measured many years before the K_n magnitudes. Quasars with flat radio spectra are known to be highly variable: this could thus introduce a scatter into the $B_J - K_n$ colours, though it is hard to see why it should introduce a systematic reddening.
- Elliptical galaxies with redshifts $z > 0.1$ have very red $B_J - K_n$ colours, due to the redshifted 400nm break. If the host galaxies make a significant contribution to the integrated light from the Parkes sources, this could produce the red colours. Masci, Webster & Francis (1998), however, used spectra to show that this effect was only significant for $\sim 10\%$ of the sample.
- The B_J magnitudes were derived from COSMOS scans of UK Schmidt plates, and are subject to substantial systematic errors, which could introduce scatter into the $B_J - K_n$ colours (O'Brian, Webster & Francis, in preparation), though this too should not introduce a systematic reddening.
- Parkes quasars could have the same intrinsic colours as optically selected QSOs, but be reddened by dust somewhere along the line of sight (Webster et al. 1995).
- Flat-radio-spectrum quasars are thought to have relativistic jets: if the synchrotron emission from these jets has a very red spectrum and extended into the near-IR, it could account for the red colours (Serjeant & Rawlings 1996).

In this paper, we test Webster et al's results by obtaining much better photometry of a large sub-set of the Parkes sources. To minimise the effects of variability, all our photometry for a given source was obtained within a period of at most six days. All the data were obtained from photometrically calibrated images, and rather than relying on only two bands (B_J and K_n), we obtained photometry in every band from B to K_n .

In principle, multi-colour photometry should enable us to discriminate between the dust and synchrotron models. If quasars have intrinsically blue power-law continua (eg. $F_\nu \propto \nu^{-0.3}$, Francis 1996), reddened by a foreground dust screen with an extinction $E(B - V)$ between the B and V bands (in magnitudes) and an optical depth inversely proportional to wavelength, then the observed continuum slope will be

$$F_\lambda \propto e^{-2E(B-V)/\lambda} \lambda^{-1.7}, \quad (1)$$

where λ is the wavelength in μm . This is plotted in Fig 1. Note the very characteristic 'n' shape, as the dust absorption increases exponentially into the blue.

If, alternatively, the redness is caused by the addition of some red synchrotron emission component to the underlying blue continuum, continuum shapes will have a characteristic 'u' shape, dominated by the underlying blue flux at short wavelengths but by the new synchrotron component at longer wavelengths (Fig 2).

If radio-quiet red quasars exist, they cannot be selected by conventional optical surveys. We show that by combining optical and near-IR data, it should be possible to select any radio-quiet sources with the colours of most of our radio-selected red quasars.

This paper describes the observations, presents the data, includes some simple phenomenological analyses of the results, and discusses the colour selection of red quasars in the optical

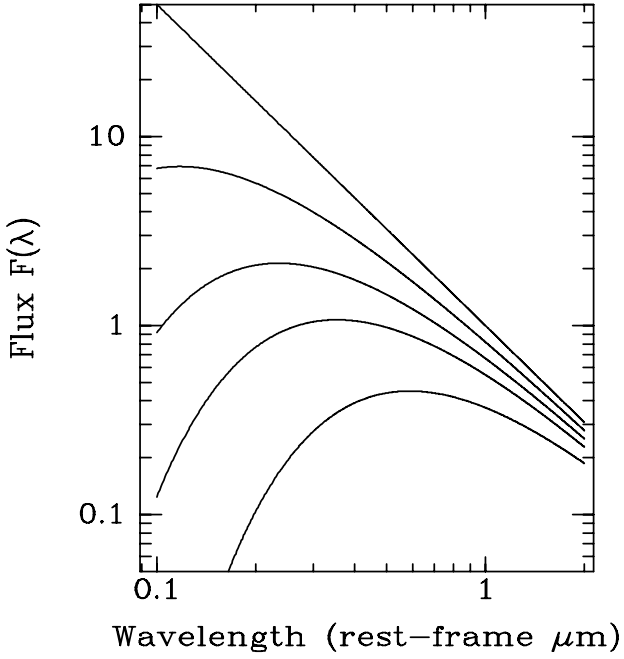


Figure 1: Continuum shapes of dust affected quasars. The extinction $E(B - V)$ increases downwards: values are 0, 0.1, 0.2, 0.3, 0.4. Note the characteristic ‘n’ shape.

and near-IR. We defer the detailed modelling of the data to another paper: Whiting, Webster & Francis (2000).

2 OBSERVATIONS

We obtained quasi-simultaneous B, V, R, I, J, H and K_n photometry of a subset of the Parkes sample. Observations were taken during 26 nights in 1997 (Table 1) at Siding Spring Observatory. Optical images were obtained with either the 1 m telescope, or with the imager on the 2.3 m telescope. Near-IR images were obtained with the CASPIR 256×256 InSb array camera (McGregor et al. 1994) on the 2.3 m telescope. 157 Parkes sources were observed in some or all of the bands, as well as a small control sample of 12 optically selected QSOs randomly selected from the Large Bright QSO survey (LBQS, Morris et al. 1991); an optical QSO survey well matched in size and redshift distribution to the Parkes sample. To minimise the effects of variability, all the observations of an individual source were made within, at most, a six day period (Table 2). Flat spectrum quasars typically vary by 10% or less on these timescales, though very occasional greater variations are seen, typically in BL Lac objects (eg. Wagner et al. 1990, Heidt & Wagner 1996). Only data taken in photometric conditions were used: seeing was typically 1–2”.

Bright objects were typically observed for \sim five minutes in each band. Fainter objects were observed for up to two hours in our most sensitive bands (R , I and H). If they were seen in these bands, we observed them in progressively bluer bands as time allowed. Four sources were not detected in any band: PKS 1535+004, PKS 1601–222, PKS 1649–062 and PKS 2047+098.

About five standard stars, spanning a range of colours, were observed each night: in the optical, the Graham E regions (Graham 1982) were used, while in the near-IR, photometric calibration was obtained using the IRIS standard stars, which have magnitudes on the Carter SAAO system

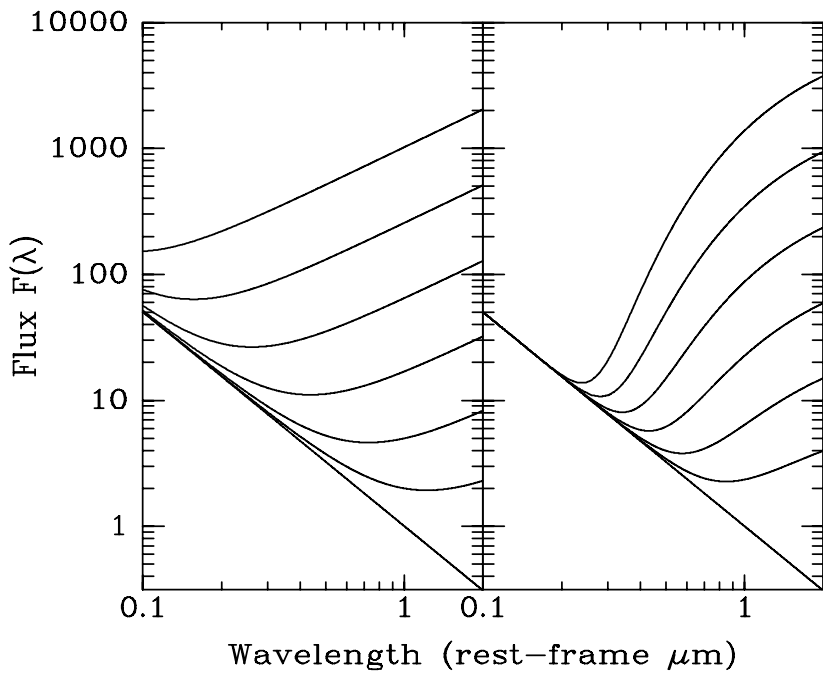


Figure 2: Continuum shapes of quasars with an additional red emission component. To show some of the possibilities, two different arbitrary functional forms have been chosen for the red component: a power-law (left) and an exponential (right). The strength of this red component increases upwards. Note the characteristic ‘u’ shape. The plausibility of synchrotron models is discussed in Whiting, Webster & Francis (2000).

Table 1: Observing Log

Night Code	Date	Telescope/Instrument
A	April 12, 1997	1m
B	April 13, 1997	1m
C	April 14, 1997	2.3m Imager
D	April 15, 1997	2.3m Imager
E	April 16, 1997	2.3m Caspir
F	April 17, 1997	2.3m Caspir
I	July 12, 1997	1m
J	July 13, 1997	1m
K	July 14, 1997	1m
L	July 13, 1997	2.3m Imager
M	July 14, 1997	2.3m Imager
N	July 15, 1997	2.3m Caspir
O	July 16, 1997	2.3m Caspir
P	July 17, 1997	2.3m Caspir
Q	July 18, 1997	2.3m Caspir
R	July 19, 1997	2.3m Caspir
S	July 20, 1997	2.3m Caspir
T	Sept 7, 1997	1m
U	Sept 8, 1997	1m
V	Sept 9, 1997	2.3m Imager
W	Sept 10, 1997	2.3m Imager
X	Sept 11, 1997	2.3m Caspir
Y	Sept 12, 1997	2.3m Caspir
Z	Sept 13, 1997	2.3m Caspir

(Carter & Meadows 1995). Within individual nights, the scatter in photometric zero points (without using colour corrections) was $< 3\%$ rms, so all the standards in a given band were simply averaged to give the final calibration.

All 98 Parkes sources lying in the RA. ranges 00:36 – 00:57, 01:53 – 02:40 and 14:50 – 22:52 (B1950) were observed in both the optical and the IR: these should thus form an unbiased, complete sub-sample of the whole Parkes Half-Jansky sample. The remaining 59 sources were selected for observation mainly on the basis of prevailing weather conditions, and so should also form a reasonably unbiased sub-sample. No selection was made against radio galaxies: sources with resolved optical or near-IR images (as classified by the COSMOS plate measuring machine from UK Schmidt plates, and checked by visual inspection of our images) are listed in Table 2. Where appropriate, they are excluded from the following analysis.

Optical images were bias- and overscan-subtracted, and then flat fielded using twilight sky flats. For the fainter sources, multiply dithered 300- or 600-second exposures were taken: these were combined using inverse variance weighting. The infrared exposures were made up of multiple dithered 60 second images, each made up of two averaged 30 sec exposures in J , six averaged 10 sec exposures in H and twelve averaged 5 sec exposures in K_n . These were bias- and dark-subtracted, and then corrected for the non-linearity of the CASPIR detector using a simple quadratic correc-

tion term (derived from plots of median counts against exposure time obtained from dome flats). Known bad pixels were replaced by the interpolated flux from neighbouring pixels. Flat fields were obtained by taking exposures of the dome with lamps on and off, and subtracting one from the other: this removes the contribution from telescope emission, and substantially improves the photometric accuracy attainable. Individual images were sky subtracted, using a median of the 10 images taken nearest in time. The dithered images were then aligned and combined, using the median to remove residual errors.

The radio sources were identified from the radio positions by using astrometry from nearby stars, bootstrapped from positions in the COSMOS/UKST and APM/POSS sky catalogues, maintained on-line at the Anglo-Australian Observatory. Magnitudes were then measured using circular apertures, with the sky level determined from the median flux in an annulus around the sky aperture. For unresolved sources, the photometric apertures were set by the seeing: typical aperture radii were $\sim 5''$. For resolved sources (mostly low redshift radio galaxies) larger circular apertures were used, centred on the galactic nucleus. These larger aperture radii are listed in the footnotes to Table 2. Standard stars were measured with similar aperture sizes.

Quoted errors are the sum (in quadrature) of random errors and an assumed 5% error in the photometric zero points. Random errors were determined by measuring the rms (root-mean-squared) pixel-to-pixel variation in sky regions, and scaling to the aperture size used. This will be accurate for fainter (sky or read-noise limited) sources, but will underestimate random errors for the brightest few sources. The photometric zero point errors were estimated from the scatter in zero points between different standard star measurements in an individual night: typical rms scatters are $< 3\%$, so we adopted a conservative value of 5% as our zero point error.

For modelling and plotting purposes, we converted the magnitudes into fluxes. We assumed fluxes for zero magnitude objects as listed in Table 3. In the optical, our filter set approximate the Johnson & Cousins system, and were calibrated using the Graham standards (also approximating Johnson & Cousins). The zero magnitude star fluxes for this system were taken from Bessell Castelli & Plez (1998). In the infrared, our observations used the CASPIR filter set calibrated by the IRIS standards. Zero magnitude fluxes were calculated by P. McGregor, assuming that Vega is well represented in the near-IR by a black body of temperature 11200 K, and normalisation $F_\lambda(555\text{nm}) = 3.44 \times 10^{-12} \text{W cm}^{-2}\mu\text{m}^{-1}$ (Bersanelli, Bouchet & Falomo 1991). These normalisations agree closely with those quoted for UKIRT near-IR standards (MacKenty et al. 1997). Our observations were made with the K_n filter, but were calibrated using the quoted K magnitudes of the IRIS standards without applying a colour correction term, and should thus be normalised to a K -band zero point.

3 Results and Discussion

3.1 The Colour Distribution

The results are listed in Table 4. Quoted errors are 1σ ; upper limits are 3σ .

Our data confirm the basic result of Webster et al: the Parkes quasars have very different $B - K$ colours from optically selected QSOs (Fig 3). The difference is significant: a Kolmogorov-Smirnov test shows that the probability of getting two samples this different from the same parent population is only 9.1×10^{-5} . The bluest Parkes sources have colours very similar to those of optically selected QSOs, but the distribution of colours extends much further into the red.

Table 3: Assumed Fluxes of a Zero Magnitude Star

Filter	Mean Wavelength (μm)	Flux of Zero Magnitude Star (F_λ , $\text{W m}^{-2}\text{nm}^{-1}$)
B	0.440	6.32×10^{-11}
V	0.550	3.64×10^{-11}
R	0.700	2.18×10^{-11}
I	0.880	1.13×10^{-11}
J	1.239	3.11×10^{-12}
H	1.649	1.15×10^{-12}
K	2.132	4.10×10^{-13}

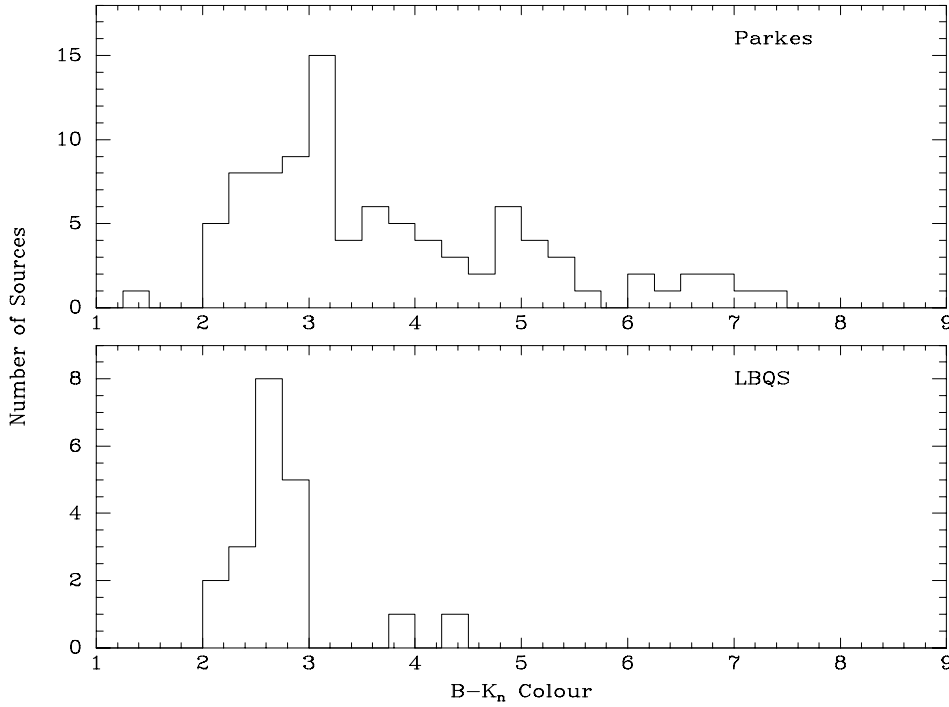


Figure 3: The distribution of $B - K_n$ colours for the Parkes sample (top panel), and the optically selected LBQS sample (bottom panel). Sources with spatially extended images (radio galaxies) have been excluded, as have sources with redshift $z > 3$ (as Ly α forest depressed the B -band flux). Only Parkes sources within the complete sub-sample have been used. The LBQS data from this paper have been supplemented by data from Francis (1996).

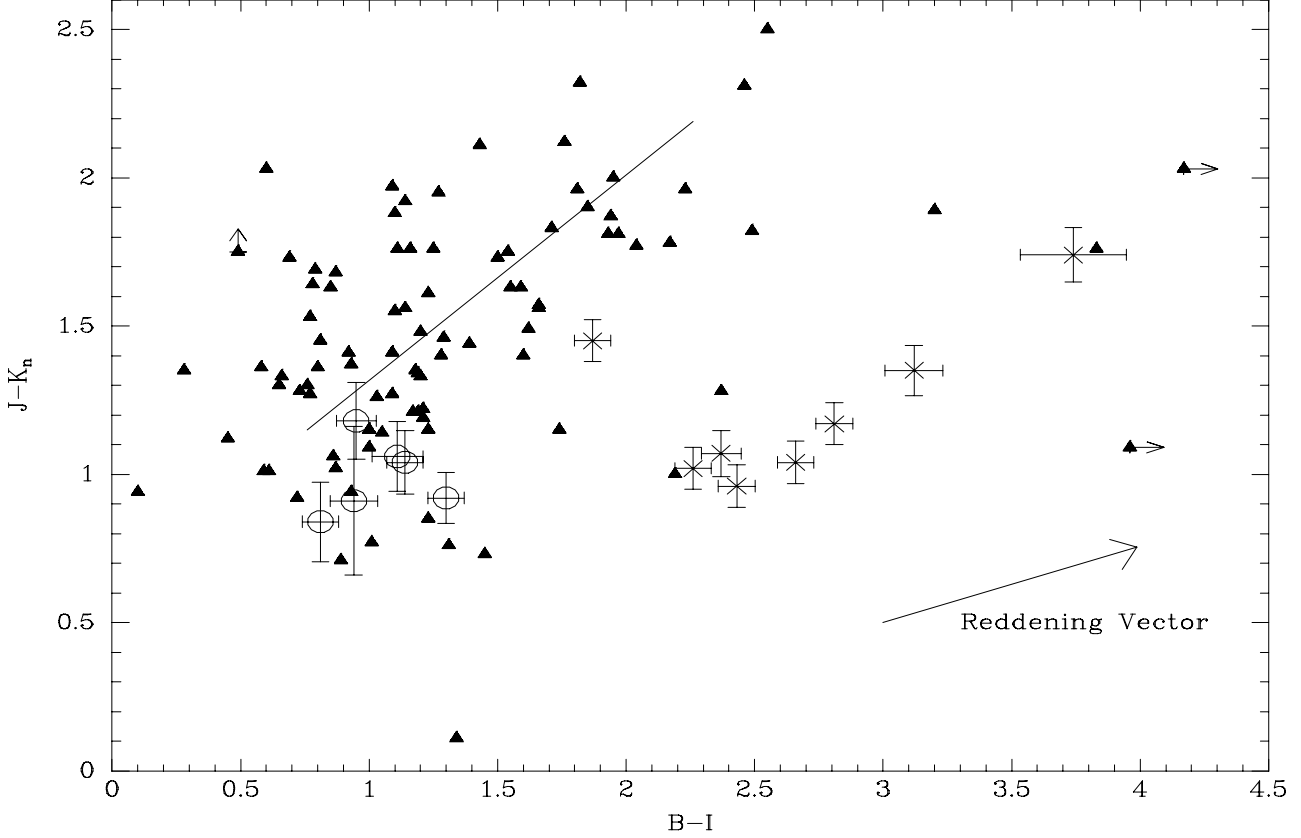


Figure 4: The optical and infra-red colours of the complete sub-set of the Parkes sample (triangles and crosses), compared with a small sample of optically selected LBQS QSOs (circles). Solid triangles denote unresolved sources: crosses are galaxies. The solid line shows where a pure power-law continuum slope would lie: it runs from $F_\nu \propto \nu^0$ on the left end, to $F_\nu \propto \nu^{-2}$ on the right end. Error bars are not shown for the unresolved Parkes sources, but are comparable to those of the optically selected QSOs. The reddening vector is for an extinction $E(B - V) = 0.2$, a redshift of one, and dust extinction as in equation 1. The direction of the reddening vector is independent of redshift.

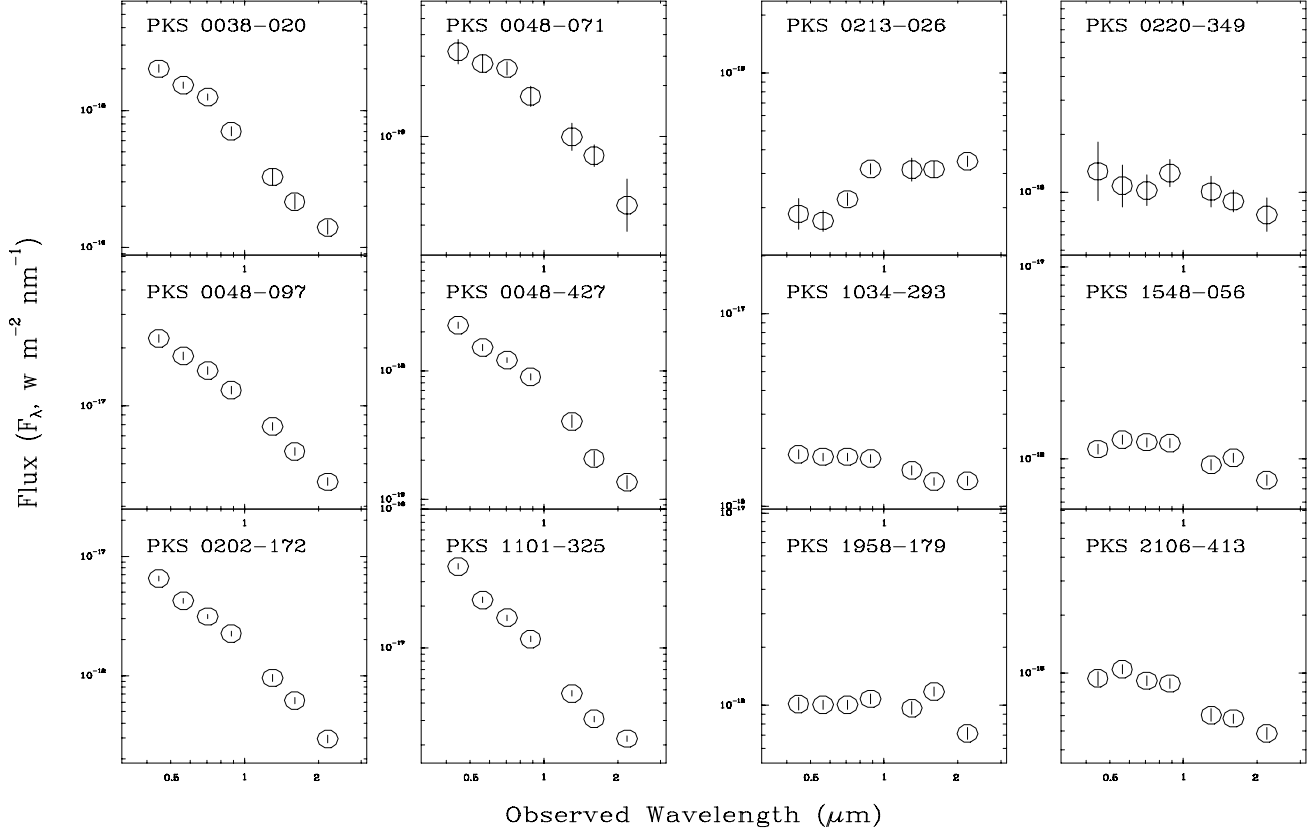


Figure 5: Spectral energy distributions of representative Parkes quasars from the blue (left six plots) and red (right six plots) ends of the ‘main sequence’, as defined in the text. Sources on the left have $J - K_n < 1.5$ and $B - I < 1.5$; sources on the right have $J - K_n > 1.8$ and $3 > B - I > 1.8$.

3.2 The ‘Main Sequence’

Are the Parkes sources uniformly red everywhere between B and K_n ? In Fig 4 we plot a measure of the optical colour ($B - I$) against a measure of the near-IR colour ($J - K_n$) for the complete sub-sample. Objects whose continuum shape approximates a featureless power-law all the way from B to K_n should lie close to the solid line in this plot.

~ 90% of all the Parkes sources do indeed lie close to the power-law line in Fig 4. These sources form a ‘main sequence’ of quasar colours, stretching from blue objects with $F_\nu \propto \nu^0$ to red objects with $F_\nu \propto \nu^{-2}$. Examples of quasars from both ends of this ‘main sequence’ are shown in Fig 5. Note that these quasars can lie on either side of the power-law line: ie. they can have both ‘n’- and ‘u’-shaped continuum spectra. The majority, however, lie above the line, consistent with slightly ‘u’-shaped spectra (redder in the near-IR than in the optical). This supports the synchrotron model for these sources. We defer discussion of this point to the detailed synchrotron modelling of the companion paper Whiting et al.

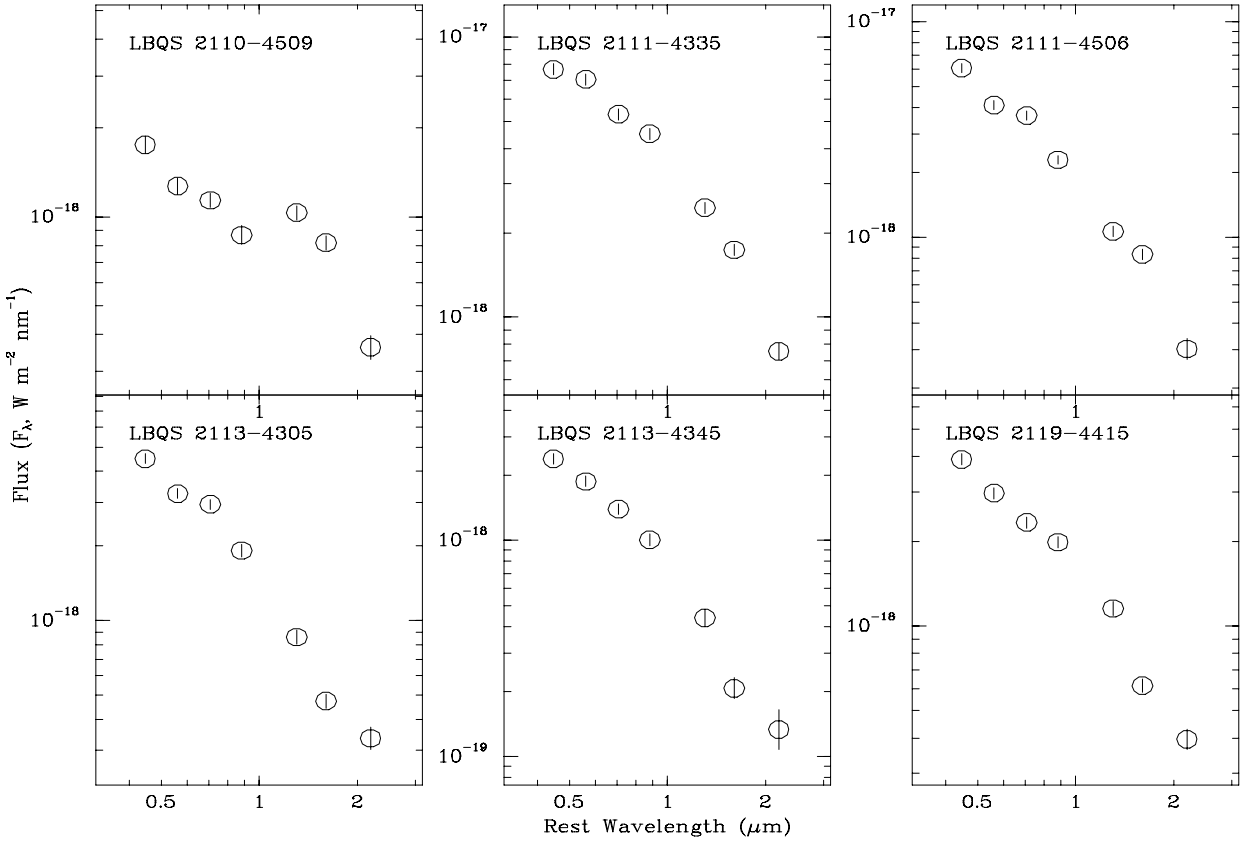


Figure 6: Spectral energy distributions of all six optically selected QSOs with complete photometric data.

3.3 Optically Selected QSOs

As Fig 4 shows, the optically selected QSOs all have very similar colours, and lie at the blue end of the ‘main sequence’. They lie systematically below the power-law line, however, indicating that they have ‘n’ shaped spectra: ie. they are redder in the optical than in the near-IR. This can be seen in their spectra energy distributions, shown in Fig 6.

This spectral curvature matches the predictions of the dust model. Wills, Netzer & Wills (1985), however, suggested that it may be partially due to blended Fe II and Balmer-line emission, though Francis et al. (1991) argued that this curvature is too large to be plausibly explained by emission-line contributions.

The position of the optically selected QSOs at the blue end of the ‘main sequence’ would be expected if the cause of redness in the Parkes quasars is the addition of a red synchrotron component to an underlying blue continuum which is identical to that in radio-quiet QSOs (Whiting et al.).

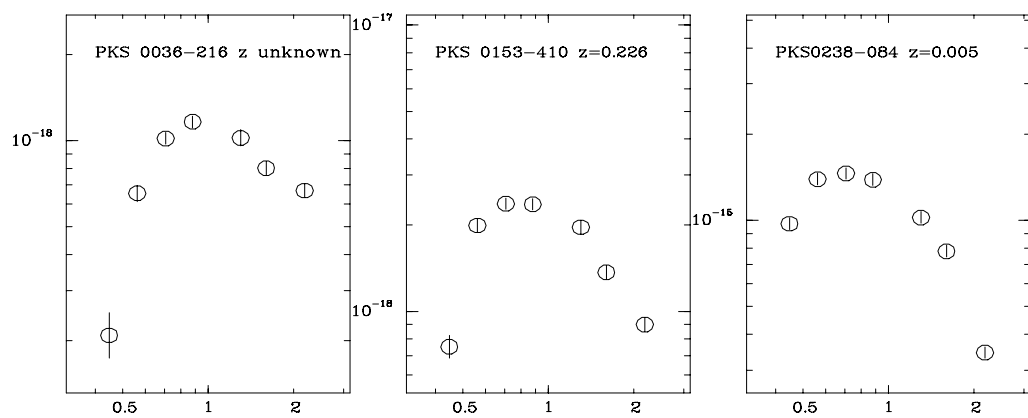


Figure 7: The spectral energy distributions of three representative galaxies from the Parkes sample.

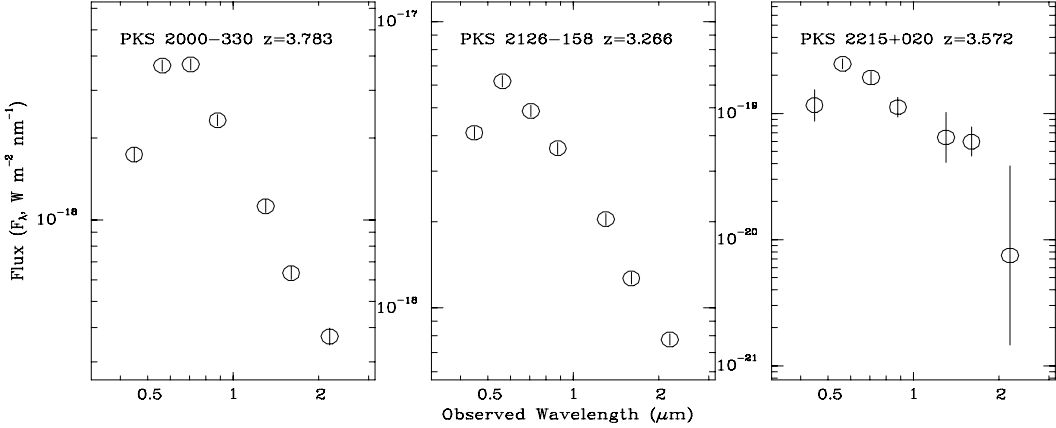


Figure 8: The spectral energy distributions of three representative Parkes quasars with redshifts $z > 3$, showing the dip in the B -band caused by Ly α forest absorption.

3.4 Galaxies and Extremely Red Objects

The colours of the spatially extended sources in the Parkes sample are sharply peaked in the red, as would be expected from moderate redshift galaxies (Fig 7). They therefore lie far below the ‘main sequence’ in Fig 4, the one exception being PKS 1514–241, which is a galaxy at $z=0.049$ with a BL Lac nucleus, which is presumably diluting the galaxy colours. Higher redshift galaxies lie further to the right on this plot, as would be expected due to the 400 nm break reducing the B -band flux.

What are the other, red, highly ‘n’-shaped objects lying far below the ‘main sequence’ which are not spatially resolved? A few are high redshift QSOs, in which the B -band flux has been reduced by Ly α forest absorption (Fig 3.4). The reddest objects, however, with $B - I > 3$ (Fig 9), do not lie at high redshifts. We have obtained spectra of four of these very red objects (Francis et al. 2000, in preparation). Three show hybrid spectra: they look like galaxies at short wavelengths, but at longer wavelengths a red power-law continuum component is seen, along with broad emission-lines. The ratios of H α to H β are around 20: far above those seen in normal AGN (~ 5) and evidence of substantial reddening (Fig 10). Note that these hybrid objects all have radio spectra indices near the steep spectrum cut-off of our sample, as do the galaxies in the sample.

The reddest objects are thus a heterogeneous group: some are high redshift quasars, some are galaxies, and some are heavily dust-reddened quasars.

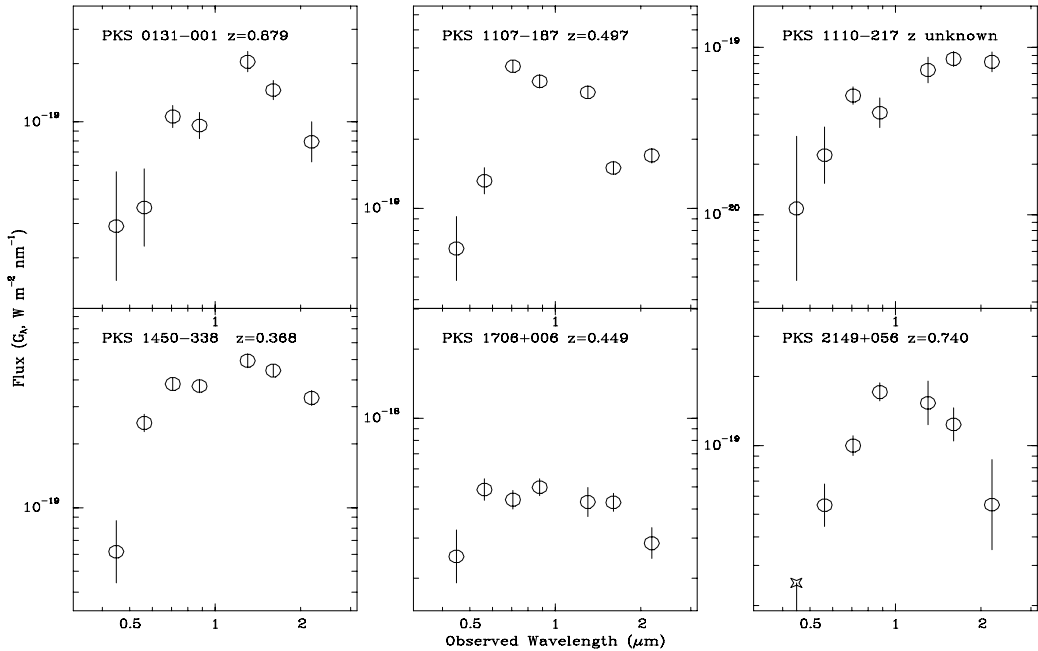


Figure 9: The spectral energy distributions of the six Parkes sources with $B - I > 3$. The data for PKS 1706+006 have been adjusted for galactic dust extinction of $E(B - V) = 0.23$ (Schlegel, Finkbeiner & Davis 1998), assuming a dust extinction law as described in the text.

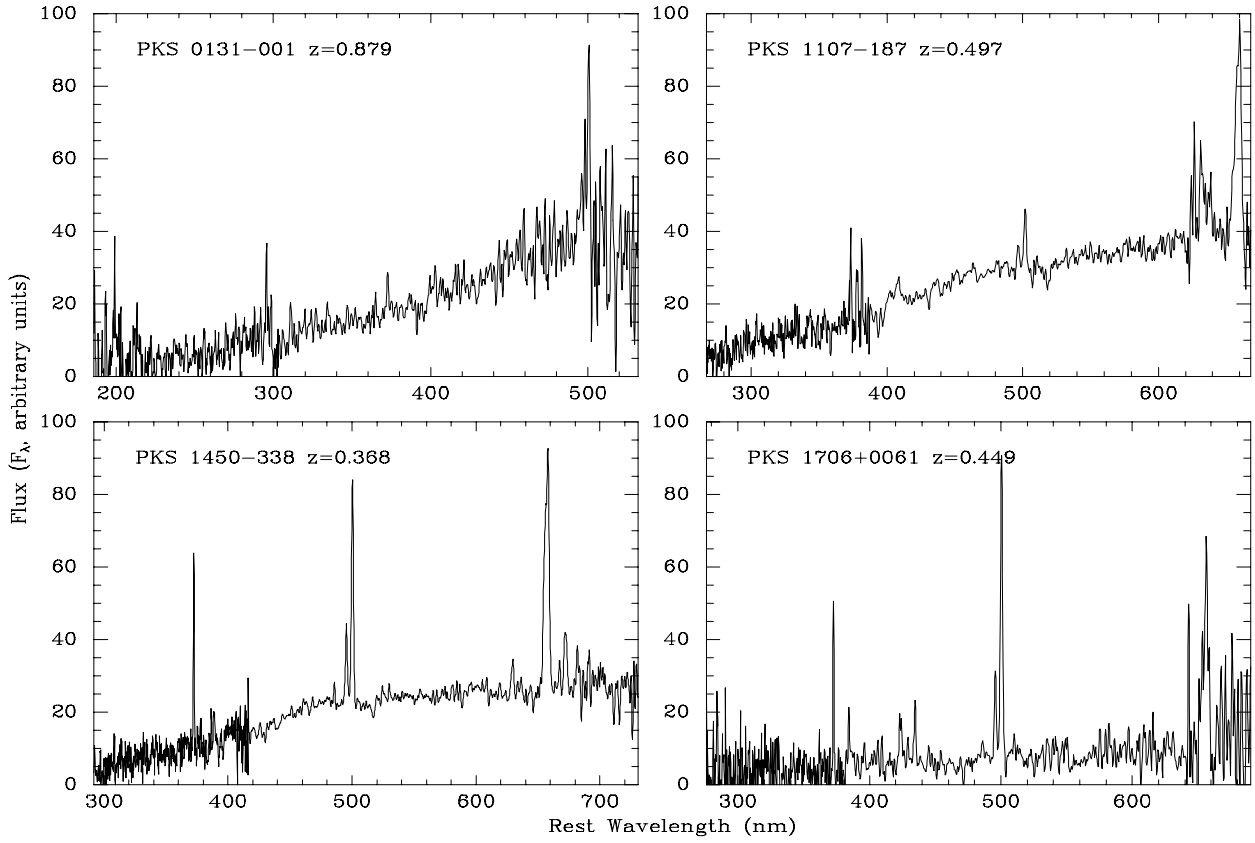


Figure 10: Optical spectra of four extremely red Parkes sources. With the exception of PKS 0131–001, the spectra show features both of galaxy light (the 400 nm break and narrow [O II] 372.7 nm and [O III] 495.9/500.7 lines) and of dust-reddened quasar light (a red continuum at long wavelengths, broad H α 656.3 nm line emission, and the notable weakness of the broad H β 486.1 nm line with respect to H α).

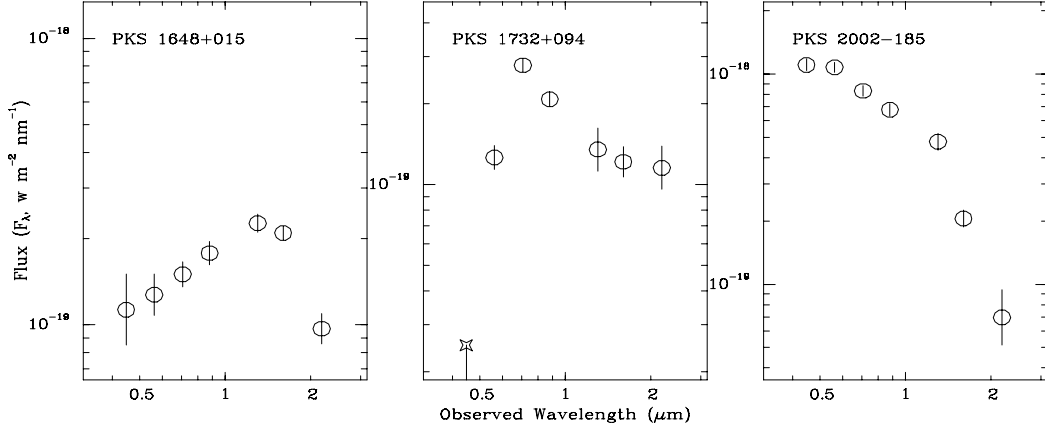


Figure 11: Spectral energy distributions of three anomalous Parkes sources.

3.5 Unidentified Objects

Four Parkes sources were not detected in any band. After correction for galactic foreground absorption (Schlegel et al.), our non-detections impose 3σ upper limits of $H > 19.61$ for PKS 1532+004, $H > 19.76$ & $K > 19.29$ for PKS 1601–222, $H > 17.22$ and $K > 16.61$ for PKS 1649–062 (which is subjected to substantial galactic reddening) and $H > 19.82$ for PKS 2047+098.

If unified schemes for radio-loud AGN are correct, the host galaxies of our flat-radio-spectrum sources should be very similar to those of steep-radio-spectrum radio galaxies. This enables us to place a lower-limit on the redshift of these unidentified sources: even if their AGN light is completely obscured, we should still see the host galaxy, which should lie on the K -band Hubble diagram for radio galaxies (eg. McCarthy 1992). To be undetected at our magnitude limits, therefore, all these sources must lie above redshift 1, and apart from PKS 1649–062, probably lie above redshift 3.

3.6 Anomalous Objects

Three sources have colours that do not fit any of these categories (Fig 11). We discuss these in turn.

PKS 1648+015 shows a smooth optical power-law rising into the red, until at around $1.4\mu\text{m}$, the flux abruptly decreases. As all the IR data points were taken within minutes of each other in good weather conditions, we believe that this near-IR turn-over is real. We obtained a somewhat noisy optical spectrum of this source (Drinkwater et al.) which shows a featureless, very red power-law, in excellent agreement with the photometry. We cannot explain this source.

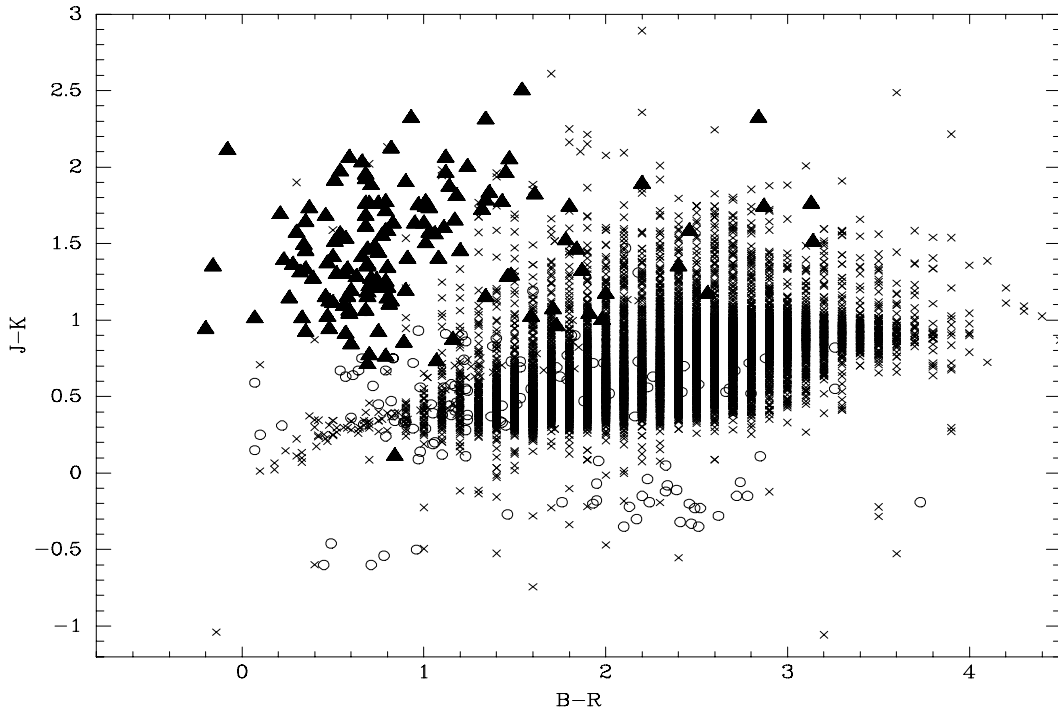


Figure 12: Optical and near-IR colours of the Parkes sources (triangles) compared to photometry of 6400 high galactic latitude point sources drawn from the 2MASS survey (crosses) and sources with $K < 22$ from the EIS Hubble Deep Field data release (circles).

PKS 1732+094 is blue longwards of around $0.6\mu\text{m}$, but drops dramatically at shorter wavelengths. Our spectrum of this source (Drinkwater et al.) is too poor to be of any use. We hypothesise that this may be a very high redshift $z > 4$ quasar, and that the drop in the blue is due to Ly α absorption.

PKS 2002–185 has optical colours typical of the bluest Parkes sources, but in the near-IR is bluer still: far bluer than any other source at these wavelengths. An optical spectrum, covering a very restricted wavelength range (Wilkes et al. 1983) shows only a single broad emission-line: on the assumption that this is Mg II (279.8 nm) a redshift of 0.859 is determined.

4 Multicolour Selection of Red Quasars

Could there be a population of radio-quiet QSOs with the same colours as our radio-loud red quasars? Webster et al. showed that it is virtually impossible to find such QSOs in any sample with a blue optical magnitude limit. In this section we ask whether red QSOs could be identified by colour selection in the red optical and near-IR.

In Fig 12, we compare the optical and near-IR colours of the Parkes sources against the colours of high galactic latitude point sources drawn from the Two-Micron All Sky Survey (2MASS, $K < 15$) and ESO Imaging Survey (EIS, $K < 22$). The ‘Main Sequence’ sources, both red and blue, are clearly separated from the foreground objects. This separation is due to their power-law spectral energy distributions: as compared to the convex spectral energy distributions of stars and

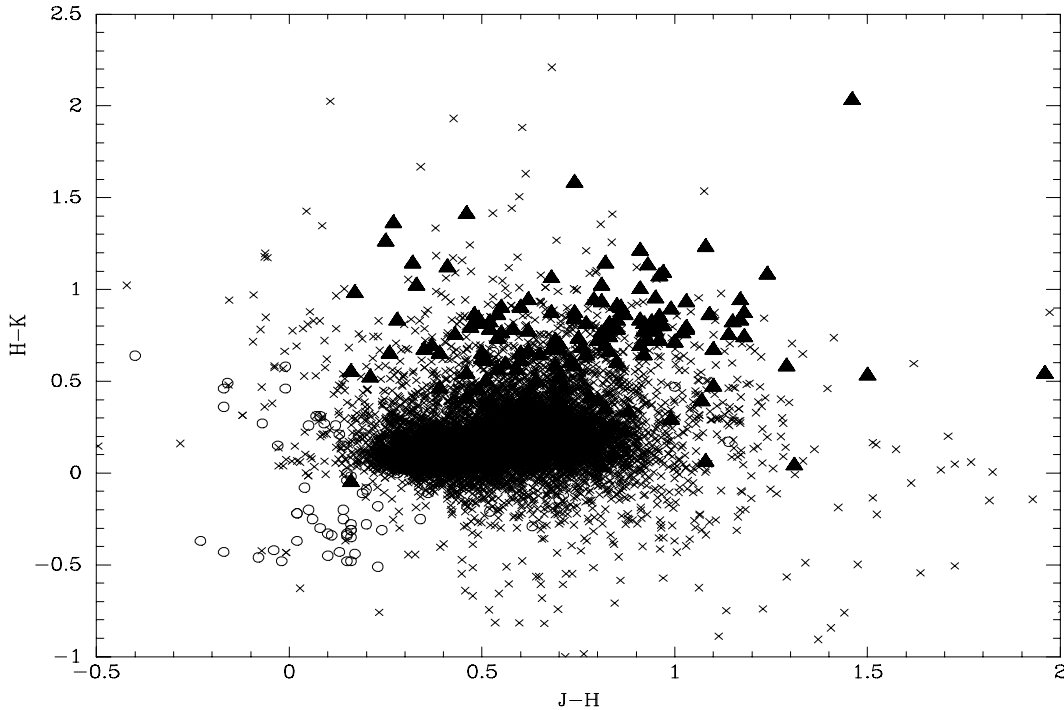


Figure 13: Near-IR colours of the Parkes sources (triangles) compared to photometry of 6400 high galactic latitude point sources drawn from the 2MASS survey (crosses) and sources with $K < 22$ from the EIS Hubble Deep Field data release (circles).

galaxies, the quasars have excess flux in B and/or K . This selection technique is similar to the ‘KX’ technique proposed by Warren, Hewett & Foltz (1999). Unfortunately, the very red sources lying below the ‘main sequence’ have colours within the stellar locus and will be hard to find.

Can red quasars be identified purely on the basis of their near-IR colours? In Fig 13, we show that most of the Parkes quasars lie in regions of the near-IR colour-colour plot with substantial stellar contamination, but that the reddest move away from the stellar locus, and could be detectable in the IR alone. Fig 14 shows that purely optical colour selection is not likely to be effective.

5 Conclusions

The Parkes quasars can, we conclude, be crudely divided into three populations:

1. **The ‘Main Sequence’:** $\sim 90\%$ of the Parkes sources have approximately power-law spectral energy distributions, with spectral indices α ($F_\nu \propto \nu^\alpha$) in the range $0 > \alpha > -2$. The nature of these sources is discussed by Whiting et al.
2. **Very Red Sources:** These sources, which comprise $\sim 10\%$ of the Parkes sample, are characterised by much redder continuum slopes in the optical than in the IR. They tend to have relatively steep radio spectra. Half these sources are radio galaxies, while most of

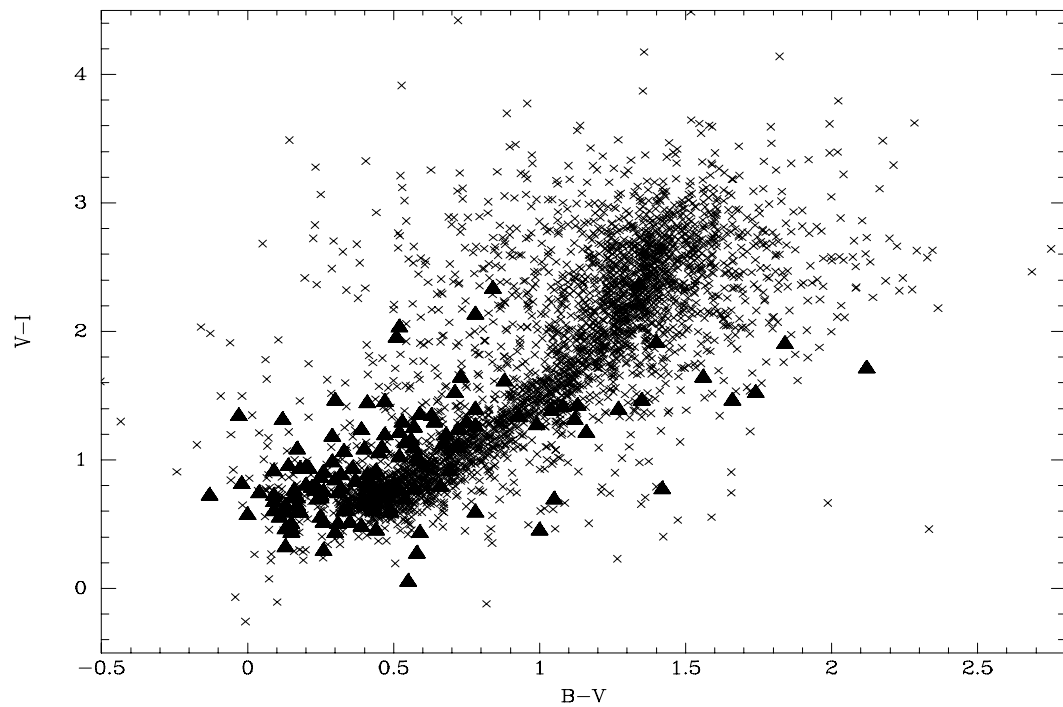


Figure 14: Optical colours of the Parkes sources (triangles) compared to photometry of 3200 high galactic latitude point sources drawn from the EIS wide survey (crosses).

the remainder are highly dust-reddened quasars. The undetected sources are probably high redshift members of this class.

3. Oddballs:

Roughly 2% of the Parkes sample defy this categorisation.

The ‘main sequence’ sources, both red and blue, should be easily detectable in combined near-IR and optical QSO surveys, due to their excess flux in the K and/or B bands.

Acknowledgements

We wish to thank Mike Bessell and Peter MacGregor for their help with the details of the photometry, and Tori Ibbetson for her assistance with the observations. This publication makes use of data products from the Two Micron All Sky Survey, which is a joint project of the University of Massachusetts and the Infrared Processing and Analysis Center, funded by the National Aeronautics and Space Administration and the National Science Foundation, and of catalogues from the ESO Imaging Survey, obtained from observations with the ESO New Technology Telescope at the La Silla observatory under program-ID Nos 59.A-9005(A) and 60.A-9005(A).

References

- Bersanelli, M., Bouchet, P., & Falomo, R. 1991, A & A, 252, 854
 Bessell, M. S., Castelli, F., & Plez, B. 1998, A & A, 333, 231
 Carter, B. S., & Meadows, V. S. 1995, MNRAS, 276, 734
 Drinkwater, M. J., Webster, R. L., Francis, P. J., Condon, J. J., Ellison, S. L., Jauncey, D. L., Lovell, J., Peterson, B. A., & Savage, A. 1997, MNRAS, 284, 85
 Francis, P. J., Hewett, P. C., Foltz, C. B., & Chaffee, C. B., 1991, ApJ 373, 465
 Francis, P. J. 1996, Publ. Astron. Soc. Australia, 13, 212
 Graham J. A. 1982, PASP 94, 265
 Heidt, J. & Wagner, S.J. 1996, A & A, 305, 42
 Ledden, S.E. & O'Dell, S.L. 1983, ApJ, 270, 434
 MacKenty, J. W. et al, 1997, “NICMOS Instrument Handbook”, Version 2.0, (Baltimore: STScI)
 Masci, F. J., Webster, R. L. & Francis, P. J. 1998, MNRAS 301, 975
 McCarthy, P. 1992, Ann Rev A & A, 31, 639
 McGregor, P., Hart, J., Downing, M., Hoadley, D., & Bloxham, G. 1994, in Infrared Astronomy with Arrays: The Next Generation, ed. I. S. McLean (Kluwer: Dordrecht), p. 299
 Morris S. L., Weymann R. J., Anderson S. F., Hewett P. C., Foltz C. B., Chaffee F. H. & Francis P. J. 1991, AJ, 102, 1627
 Neugebauer, G., Green, R. F., Matthews, K., Schmidt, M., Soifer, B. T., & Bennet, J. 1987, ApJS, 63, 615
 Rieke, G.H., Lebofsky, M.J. & Wisniewski, W.A. 1982, ApJ 263, 73
 Schlegel, D. J., Finkbeiner, D. P., & Davis, M. 1998, ApJ 500, 525
 Serjeant, S., & Rawlings, S. 1997, Nature, 379, 304
 Stickel, M., Rieke, G.H., Kühr, H. & Rieke, M.J. 1996, ApJ, 468, 556
 Wagner, S.J., Sanchez-Pons, F., Quirrenbach, A., & Witzel, A. 1990, A & A, 235 L1
 Warren, S.J., Hewett, P.C. & Foltz, C.B. 1999, MNRAS in press (astro-ph/9911064).
 Webster, R. L., Francis, P. J., Peterson, B. A., Drinkwater, M. J., & Masci, F. J. 1995, Nature, 375, 469
 Whiting, M.T., Webster, R.L. & Francis, P.J. 2000, MNRAS submitted.

Wilkes, B. J., Wright, A. E., Jauncey, D. L. & Peterson, B. A., 1983, PASA, 5, 2
Wills, B., Netzer, H., & Wills, D. 1985, ApJ 288, 94

TABLE 2
OBSERVATION DATES AND EXPOSURE TIMES

Name	Redshift z	Morpho- logy	B	V	R	I	J	H	K _n		
PKS 0036-216	...	galaxy	W	600	W	300	W	300	X	240	
PKS 0038-020	1.178	faint	U	360	U	360	U	360	X	240	
PKS 0048-071	1.974	point	W	300	W	300	W	300	X	1200	
PKS 0048-097	...	point	W	180	W	180	W	180	X	1200	
PKS 0048-427	1.749	point	W	300	W	300	W	300	X	1200	
PKS 0056-001	0.717	point	U	300	U	300	U	300	...	1200	
PKS 0131-001	0.879	faint	M	1200	M	600	M	600	N	1200	
PKS 0153-410	0.226	galaxy	V	300	V	180	V	180	X	1200	
PKS 0202-172	1.740	point	V	180	V	180	V	180	X	1200	
PKS 0213-026	1.178	faint	V	600	V	600	V	600	X	1200	
PKS 0216+011	1.610	faint	V	300	V	300	V	300	X	1200	
PKS 0220-349	1.490	faint	V	300	V	300	V	300	X	1200	
PKS 0221+067	0.510	point	V	300	V	300	V	300	Z	240	
PKS 0226-038	2.066	point	V	180	V	180	V	180	Z	240	
PKS 0229-398	1.646	point	V	600	V	600	V	600	Z	1200	
PKS 0232-042	1.437	point	V	180	V	180	V	180	Z	240	
PKS 0237+040	0.978	point	W	300	W	180	W	180	Z	240	
PKS 0238-084	0.005	galaxy ^a	W	60	W	60	W	60	Z	300	
PKS 0240-060	1.800	point	W	180	W	180	W	180	Z	240	
PKS 0240-217	0.314	galaxy ^b	W	180	W	180	W	180	...	300	
PKS 0256+075	0.895	point	W	960	W	600	W	600	...	0	
PKS 0301-243	...	point	W	180	W	180	W	180	...	0	
PKS 0316-444	0.076	galaxy	W	180	W	180	W	180	...	0	
PKS 0537-441	0.893	point	A	300	A	300	A	300	F	240	
PKS 0829+046	...	point	A	300	A	300	A	300	F	240	
PKS 0912+029	0.427	point	C	600	C	300	C	300	E	1200	
PKS 0922+005	1.717	point	D	300	D	300	...	0	
PKS 1016-311	0.794	point	B	300	B	300	B	300	F	240	
PKS 1020-103	0.197	point	A	300	A	300	A	300	F	240	
PKS 1021-006	2.549	point	B	300	B	300	B	300	F	240	
PKS 1032-199	2.198	point	B	300	B	300	B	300	F	240	
PKS 1034-293	0.312	point	B	300	B	300	B	300	F	240	
PKS 1036-154	0.525	point	C	600	C	300	C	300	F	240	
PKS 1038+064	1.264	point	A	300	A	300	A	300	...	0	
PKS 1042+071	0.698	point	B	600	B	300	B	300	...	0	
PKS 1045-188	0.595	point	B	600	B	300	B	300	F	2240	
PKS 1048-313	1.429	point	B	600	B	300	B	300	...	0	
PKS 1055-243	1.086	point	B	300	B	300	B	300	...	0	
PKS 1055+018	0.888	point	B	300	B	300	B	300	...	0	
PKS 1101-325	0.355	point	A	300	A	300	A	300	F	240	
PKS 1107-187	0.497	faint	D	2400	D	1800	D	1200	E	1200	
PKS 1110-217	...	faint	C	2400	C	2400	C	1800	E	1200	
PKS 1133-172	1.024	faint	D	1800	D	1200	D	1200	E	240	
PKS 1136-135	0.557	point	A	300	A	300	A	300	F	240	
PKS 1156-094	...	faint	C	600	C	600	C	600	F	1200	
PKS 1244-255	0.638	point	A	300	A	300	A	300	F	240	
PKS 1256-229	1.365	point	A	300	A	300	A	300	F	240	
PKS 1313-333	1.210	point	A	300	A	300	A	300	F	240	
PKS 1330+022	0.216	galaxy	A	600	A	300	A	300	F	240	
PKS 1353-341	0.223	galaxy ^c	A	1200	A	300	A	300	F	240	
PKS 1404-342	1.122	point	K	300	K	300	K	300	O	240	
PKS 1411+094	0.162	galaxy ^d	K	300	K	300	K	300	O	1200	
PKS 1430-155	1.573	faint	L	1800	L	1800	L	1200	O	2400	
PKS 1430-178	2.326	point	J	300	J	300	J	300	P	240	
PKS 1435-218	1.187	point	J	300	J	300	J	300	P	240	
PKS 1437-153	0.254	point	J	300	J	300	J	300	P	240	
PKS 1438-347	1.159	point	J	300	J	300	J	300	P	240	
PKS 1450-338	0.368	faint	D	2400	D	1200	D	600	E	240	
PKS 1454-060	1.249	point	I	300	I	300	I	300	P	240	
PKS 1456+044	0.394	point	C	900	C	900	E	1200	
PKS 1504-166	0.876	point	I	600	I	300	I	300	P	240	
PKS 1508-055	1.185	point	I	300	I	300	I	300	P	240	
PKS 1509+022	0.219	galaxy ^e	I	300	I	300	P	240	
PKS 1510-089	0.362	point	A	300	A	300	A	300	E	240	
PKS 1511-100	1.513	point	B	300	B	300	B	300	F	240	
PKS 1511-210	1.179	point	L	900	L	600	L	600	Q	240	
PKS 1514-241	0.049	galaxy ^f	B	300	B	60	B	60	P	240	
PKS 1518+045	0.052	galaxy ^g	K	300	K	300	K	300	P	240	
PKS 1519-273	0.510	point	K	300	K	300	K	300	P	240	
PKS 1532+016	1.435	point	K	300	K	300	K	300	P	240	
PKS 1535+004	3.497	faint	M	600	...	M	2400	M	2400	...	0
PKS 1542+042	2.184	point	J	300	J	300	J	300	Q	240	
PKS 1546+027	0.415	point	A	300	A	300	A	300	F	240	
PKS 1548+056	1.422	point	K	900	K	300	K	300	Q	240	
PKS 1550-269	2.145	point	B	300	B	300	B	300	F	1200	
PKS 1555-140	0.097	galaxy ^h	J	300	J	300	J	300	Q	240	
PKS 1555+001	1.770	faint	M	600	M	600	M	300	Q	240	
PKS 1556-245	2.818	point	I	360	I	360	I	300	Q	240	
PKS 1601-222	...	faint	L	2400	L	2400	...	3600	
PKS 1602-001	1.624	point	J	300	J	300	J	300	O	240	
PKS 1614+051	3.217	point	K	900	K	600	K	900	O	240	
PKS 1615+029	1.341	point	A	300	AD	2100	AD	900	E	1200	
PKS 1616-063	2.088	point	J	300	J	300	J	300	O	240	
PKS 1635-035	2.856	point	D	600	D	600	D	600	F	2240	
PKS 1648+015	...	faint	C	600	C	600	C	600	E	1200	
PKS 1649-062	...	faint	C	3000	C	2400	F	2240	
PKS 1654-020	2.000	faint	M	1800	M	1800	M	1800	Q	1200	
PKS 1655+077	0.621	point	V	600	V	600	V	300	Y	240	
PKS 1656+053	0.887	point	I	300	I	300	I	300	P	240	
PKS 1705+018	2.576	point	I	300	I	300	I	300	Q	240	
PKS 1706+006	0.449	faint	V	1200	V	600	V	300	X	240	
PKS 1725+044	0.296	point	A	600	A	300	A	300	E	1200	
PKS 1732+094	...	faint	M	1800	L	1200	L	1200	P	1200	
PKS 1933-400	0.965	point	A	300	A	300	A	300	F	240	
PKS 1953-325	1.242	point	I	300	I	300	I	300	N	240	
PKS 1954-388	0.626	point	I	300	I	300	I	300	N	240	

TABLE 2—Continued

Name	Redshift z	Morph- ology	B	V	R	I	J	H	K _n	
Letters indicate observation dates, numbers are exposure times (seconds)										
PKS 1958–179	0.652	point	I	300	I	300	I	300	N	240
PKS 2000–330	3.783	point	I	300	I	300	I	300	P	1200
PKS 2002–185	0.859	point	B	600	B	300	B	300	E	240
PKS 2004–447	0.240	point	A	300	A	300	A	300	F	240
PKS 2008–159	1.178	point	I	300	I	300	I	300	N	240
PKS 2021–330	1.471	point	J	300	I	300	I	300	NQ	480
PKS 2022–077	1.388	point	J	600	J	600	J	600	N	240
PKS 2037–253	1.574	point	J	300	J	300	J	300	O	240
PKS 2044–168	1.937	point	J	300	J	300	J	300	N	240
PKS 2047+098	...	faint	VW	1800	W	4200	...	0
PKS 2053–044	1.177	point	J	300	J	300	J	300	O	240
PKS 2056–369	...	faint	M	2400	L	1800	O	1200
PKS 2058–135	0.029	galaxy ⁱ	J	120	J	30	J	30	Q	240
PKS 2058–297	1.492	point	J	300	J	300	J	300	P	480
PKS 2059+034	1.012	point	J	300	J	300	J	300	Q	240
PKS 2106–413	1.055	point	J	300	J	300	J	300	Q	240
PKS 2120+099	0.932	point	T	300	T	300	T	300	X	240
PKS 2121+053	1.941	point	J	300	J	300	J	300	Q	240
PKS 2126–158	3.266	point	L	600	L	1860	L	1800	P	1200
PKS 2127–096	0.780	faint	T	600	T	300	T	300	X	240
PKS 2128–123	0.499	point	K	300	K	300	K	300	O	1200
PKS 2131–021	1.285	point	K	900	K	300	K	300	Q	240
PKS 2134+004	1.937	point	K	300	K	300	K	300	Q	240
PKS 2135–248	0.821	point	K	300	K	300	K	300	Q	240
PKS 2140–048	0.344	point	K	300	K	300	K	300	Q	240
PKS 2143–156	0.698	point	K	300	K	300	K	300	Q	240
PKS 2144+092	1.113	point	T	300	T	300	T	300	X	240
PKS 2145–176	2.130	point	T	300	T	300	T	300	X	240
PKS 2145+067	0.999	point	V	120	V	120	U	300	X	240
PKS 2149–307	2.345	point	T	300	T	300	T	300	X	240
PKS 2149+056	0.740	faint	M	1800	M	1800	M	600	Q	240
PKS 2149+069	1.364	point	V	120	V	120	V	120	X	240
PKS 2155–152	0.672	point	M	1200	M	1200	M	1800	Q	1200
PKS 2200–238	2.120	point	T	300	T	300	T	300	Y	240
PKS 2203–188	0.619	point	T	300	T	300	T	300	Y	240
PKS 2206–237	0.086	galaxy ^j	V	120	V	120	V	120	Y	240
PKS 2208–137	0.392	point	V	120	V	120	V	120	Y	240
PKS 2210–257	1.833	point	V	120	V	120	V	120	Y	240
PKS 2212–299	2.703	point	V	120	V	120	V	120	Y	240
PKS 2215+020	3.572	point	V	600	V	600	V	300	Y	360
PKS 2216–038	0.901	point	L	600	L	600	L	1860	P	1200
PKS 2223–052	1.404	point	V	120	V	120	V	120	Z	240
PKS 2227–088	1.561	point	V	120	V	120	V	120	Z	240
PKS 2227–399	0.323	point	V	120	V	120	V	120	Z	240
PKS 2229–172	1.780	faint	V	600	V	600	V	300	Z	240
PKS 2233–148	0.609	point	V	600	V	300	V	300	Z	240
PKS 2239+096	1.707	point	W	300	W	300	W	300	Z	240
PKS 2240–260	0.774	point	W	180	W	180	W	180	Z	240
PKS 2243–123	0.630	point	W	180	W	180	W	180	Z	240
PKS 2245–328	2.268	point	W	180	W	180	W	180	Z	240
PKS 2245+029	...	point	W	1200	W	600	W	600	X	240
PKS 2252–090	...	faint	W	1800	W	1800	W	600	X	240
PKS 2312–319	1.323	point	J	300	J	300	J	300	O	240
PKS 2313–438	1.847	point	J	300	J	300	J	300	Q	1200
PKS 2314–409	2.448	point	J	300	J	300	J	300	Q	240
PKS 2329–415	0.671	point	J	300	J	300	J	300	Q	1200
PKS 2337–334	...	faint	L	600	L	600	L	1200	O	660
PKS 2344–192	...	faint	L M	1800	...	L	600	L	PQ	2400
PKS 2345–167	0.576	point	K	300	K	300	K	300	Q	1200
PKS 2351–154	2.675	point	K	300	K	300	K	300	Q	240
PKS 2354–117	0.960	point	K	300	K	300	K	300	Q	1200
L 2110–4509	0.555	point	U	300	U	300	U	300	Y	240
L 2111–4335	1.708	point	U	300	U	300	U	300	Y	240
L 2111–4506	1.376	point	U	300	U	300	U	300	Y	240
L 2113–4305	1.249	point	U	300	U	300	U	300	Y	240
L 2113–4345	2.053	point	U	300	U	300	U	300	Y	240
L 2113–4538	0.946	point	U	300	U	300	U	300	...	0
L 2114–4335	1.318	point	W	180	W	180	W	180	...	0
L 2114–4346	2.041	point	W	180	W	180	W	180	...	0
L 2114–4501	0.597	point	W	180	W	180	W	180	...	0
L 2116–4439	1.480	point	W	180	W	180	W	180	...	0
L 2118–4702	1.332	point	W	180	W	180	W	180	...	Z
L 2119–4415	0.728	point	W	180	W	180	W	180	Z	240

^aUse circular photometric aperture of radius 45''^bAperture radius 10''^cAperture radius 8''^dAperture radius 15''^eAperture radius 8''^fAperture radius 20''^gAperture radius 35''^hAperture radius 5''ⁱAperture radius 10''^jAperture radius 14''

TABLE 4
SOURCE MAGNITUDES

Name	B	V	R	I	J	H	K _n
PKS 0036-216	21.20 ± 0.20	19.36 ± 0.07	18.33 ± 0.05	17.46 ± 0.05	16.20 ± 0.07	15.39 ± 0.06	14.46 ± 0.06
PKS 0038-020	18.74 ± 0.07	18.44 ± 0.06	18.11 ± 0.06	18.01 ± 0.08	17.44 ± 0.15	16.82 ± 0.13	16.16 ± 0.13
PKS 0048-071	20.74 ± 0.18	20.32 ± 0.13	19.84 ± 0.10	19.53 ± 0.15	18.73 ± 0.20	17.93 ± 0.16	17.54 ± 0.39
PKS 0048-097	16.12 ± 0.05	15.75 ± 0.05	15.39 ± 0.05	14.92 ± 0.05	13.99 ± 0.05	13.24 ± 0.05	12.51 ± 0.05
PKS 0048-427	18.62 ± 0.06	18.45 ± 0.06	18.15 ± 0.05	17.75 ± 0.06	17.21 ± 0.12	16.86 ± 0.14	16.19 ± 0.13
PKS 0056-001	17.73 ± 0.05	17.55 ± 0.05	17.43 ± 0.05	...	16.49 ± 0.08	15.66 ± 0.07	14.92 ± 0.06
PKS 0131-001	23.34 ± 0.70	22.50 ± 0.50	20.78 ± 0.14	20.17 ± 0.17	17.95 ± 0.13	17.24 ± 0.12	16.78 ± 0.26
PKS 0153-410	19.81 ± 0.10	18.15 ± 0.06	17.41 ± 0.05	16.69 ± 0.05	15.49 ± 0.06	14.81 ± 0.06	14.14 ± 0.06
PKS 0202-172	17.46 ± 0.05	17.33 ± 0.05	17.11 ± 0.05	16.74 ± 0.05	16.27 ± 0.07	15.67 ± 0.07	15.35 ± 0.08
PKS 0213-026	21.33 ± 0.20	20.82 ± 0.14	19.99 ± 0.08	18.87 ± 0.07	17.48 ± 0.15	16.40 ± 0.10	15.17 ± 0.07
PKS 0216+011	20.33 ± 0.13	20.36 ± 0.13	19.54 ± 0.08	19.02 ± 0.09	18.14 ± 0.19	17.55 ± 0.12	17.33 ± 0.34
PKS 0220-349	21.73 ± 0.38	21.32 ± 0.27	20.83 ± 0.20	19.88 ± 0.18	18.72 ± 0.20	17.77 ± 0.14	16.82 ± 0.22
PKS 0221+067	19.85 ± 0.09	18.97 ± 0.06	18.24 ± 0.05	17.36 ± 0.05	16.29 ± 0.06	15.26 ± 0.06	14.47 ± 0.07
PKS 0226-038	17.56 ± 0.05	17.38 ± 0.05	17.17 ± 0.05	16.79 ± 0.05	16.40 ± 0.07	15.86 ± 0.06	15.13 ± 0.06
PKS 0229-398	19.74 ± 0.07	20.31 ± 0.10	19.90 ± 0.08	19.46 ± 0.10	18.86 ± 0.18	17.55 ± 0.12	17.51 ± 0.38
PKS 0232-042	15.73 ± 0.05	16.27 ± 0.05	15.93 ± 0.05	15.63 ± 0.05	15.22 ± 0.05	14.38 ± 0.05	14.28 ± 0.05
PKS 0237+040	18.33 ± 0.05	17.88 ± 0.05	17.53 ± 0.05	17.14 ± 0.05	16.49 ± 0.07	15.97 ± 0.07	15.15 ± 0.06
PKS 0238-084	12.03 ± 0.05	11.04 ± 0.05	10.44 ± 0.05	9.77 ± 0.05	8.70 ± 0.05	7.92 ± 0.05	7.68 ± 0.05
PKS 0240-060	19.07 ± 0.07	18.87 ± 0.07	18.61 ± 0.06	18.07 ± 0.07	17.50 ± 0.12	17.33 ± 0.16	16.35 ± 0.24
PKS 0240-217	19.20 ± 0.09	17.93 ± 0.06	17.07 ± 0.05	16.34 ± 0.05	...	14.23 ± 0.05	13.63 ± 0.06
PKS 0256+075	21.32 ± 0.18	20.68 ± 0.13	19.92 ± 0.08	18.92 ± 0.08
PKS 0301-243	16.51 ± 0.05	16.10 ± 0.05	15.69 ± 0.05	15.22 ± 0.05
PKS 0316-444	16.07 ± 0.05	14.76 ± 0.05	14.12 ± 0.05	13.51 ± 0.05
PKS 0537-441	17.93 ± 0.05	17.34 ± 0.05	16.92 ± 0.05	16.35 ± 0.05	14.76 ± 0.05	13.85 ± 0.05	13.02 ± 0.05
PKS 0829+046	16.28 ± 0.05	15.61 ± 0.05	15.11 ± 0.05	14.49 ± 0.05	13.45 ± 0.05	12.52 ± 0.05	11.80 ± 0.05
PKS 0912+029	18.75 ± 0.05	18.59 ± 0.06	18.29 ± 0.05	17.87 ± 0.06	16.97 ± 0.06	16.01 ± 0.05	15.29 ± 0.06
PKS 0922+005	17.09 ± 0.05	16.58 ± 0.05
PKS 1016-311	18.32 ± 0.06	18.01 ± 0.05	17.82 ± 0.05	17.51 ± 0.06	16.70 ± 0.08	16.42 ± 0.09	15.59 ± 0.14
PKS 1020-103	17.10 ± 0.05	16.70 ± 0.05	16.30 ± 0.05	15.62 ± 0.05	14.85 ± 0.05	14.11 ± 0.05	13.27 ± 0.05
PKS 1021-006	18.38 ± 0.06	18.25 ± 0.05	18.03 ± 0.05	17.61 ± 0.06	17.12 ± 0.10
PKS 1032-199	18.92 ± 0.06	18.83 ± 0.06	18.60 ± 0.06	18.16 ± 0.08	17.35 ± 0.12	16.80 ± 0.11	16.04 ± 0.10
PKS 1034-293	18.83 ± 0.06	18.26 ± 0.05	17.71 ± 0.05	17.01 ± 0.05	15.76 ± 0.06	14.83 ± 0.05	13.70 ± 0.06
PKS 1036-154	20.54 ± 0.11	20.07 ± 0.10	19.43 ± 0.08	18.62 ± 0.08	17.23 ± 0.11	16.32 ± 0.07	15.63 ± 0.15
PKS 1038+064	17.10 ± 0.05	16.92 ± 0.05	16.63 ± 0.05	16.43 ± 0.05
PKS 1042+071	20.38 ± 0.11	19.87 ± 0.11	19.12 ± 0.08	18.27 ± 0.08
PKS 1045-188	18.55 ± 0.05	18.26 ± 0.05	17.76 ± 0.05	17.08 ± 0.05	16.30 ± 0.07	15.30 ± 0.06	14.59 ± 0.05
PKS 1048-313	20.19 ± 0.10	20.19 ± 0.13	19.70 ± 0.11	19.21 ± 0.16
PKS 1055-243	19.13 ± 0.07	18.71 ± 0.06	18.40 ± 0.06	17.94 ± 0.07
PKS 1055+018	18.17 ± 0.05	17.63 ± 0.05	17.15 ± 0.05	16.47 ± 0.05
PKS 1101-325	15.54 ± 0.05	15.54 ± 0.05	15.31 ± 0.05	14.97 ± 0.05	14.55 ± 0.05	13.93 ± 0.05	13.16 ± 0.05
PKS 1107-187	22.44 ± 0.35	21.10 ± 0.14	19.30 ± 0.06	18.74 ± 0.07	17.46 ± 0.07	17.21 ± 0.07	15.95 ± 0.08
PKS 1110-217	24.41 ± 1.08	23.01 ± 0.42	21.57 ± 0.13	21.10 ± 0.22	19.06 ± 0.19	17.82 ± 0.11	16.74 ± 0.15
PKS 1133-172	22.32 ± 0.35	21.54 ± 0.19	20.52 ± 0.11	19.41 ± 0.09	18.37 ± 0.22	17.69 ± 0.19	16.63 ± 0.27
PKS 1136-135	16.65 ± 0.05	16.52 ± 0.05	16.39 ± 0.05	16.06 ± 0.05	15.54 ± 0.05	14.90 ± 0.05	14.40 ± 0.05
PKS 1156-094	21.95 ± 0.33	21.43 ± 0.22	20.47 ± 0.11	20.22 ± 0.17	18.16 ± 0.22	17.51 ± 0.20	16.87 ± 0.20
PKS 1244-255	17.42 ± 0.05	16.99 ± 0.05	16.63 ± 0.05	16.11 ± 0.05	15.43 ± 0.05	14.66 ± 0.05	13.85 ± 0.06
PKS 1256-229	18.43 ± 0.06	17.68 ± 0.05	17.11 ± 0.05	16.39 ± 0.05	15.16 ± 0.05	14.21 ± 0.05	13.44 ± 0.05
PKS 1313-333	18.17 ± 0.06	17.63 ± 0.05	17.16 ± 0.05	16.50 ± 0.05	15.46 ± 0.05	14.36 ± 0.05	13.69 ± 0.06
PKS 1330+022	19.02 ± 0.06	17.89 ± 0.05	17.24 ± 0.05	16.47 ± 0.05	15.23 ± 0.05	14.43 ± 0.05	13.71 ± 0.06
PKS 1353-341	19.20 ± 0.06	17.46 ± 0.05	16.74 ± 0.05	15.94 ± 0.05	15.20 ± 0.06	14.38 ± 0.05	13.62 ± 0.06
PKS 1404-342	17.37 ± 0.05	16.78 ± 0.05	16.56 ± 0.05	16.35 ± 0.05	15.67 ± 0.06	15.13 ± 0.06	14.57 ± 0.08
PKS 1411+094	18.64 ± 0.09	17.56 ± 0.06	16.77 ± 0.05	16.15 ± 0.06	15.10 ± 0.07	14.36 ± 0.06	13.78 ± 0.06
PKS 1430-155	> 22.70	23.24 ± 0.48	22.91 ± 0.48	20.73 ± 0.16	19.07 ± 0.27	17.97 ± 0.13	17.50 ± 0.37
PKS 1430-178	19.14 ± 0.07	18.92 ± 0.06	18.55 ± 0.06	18.14 ± 0.08	17.75 ± 0.24	16.78 ± 0.17	15.69 ± 0.23
PKS 1435-218	19.20 ± 0.07	18.54 ± 0.06	18.04 ± 0.05	17.75 ± 0.06	17.64 ± 0.22	17.18 ± 0.23	16.77 ± 0.53
PKS 1437-153	19.94 ± 0.11	19.01 ± 0.07	18.47 ± 0.06	17.68 ± 0.06	16.29 ± 0.08	15.11 ± 0.06	14.24 ± 0.08
PKS 1438-347	17.80 ± 0.05	17.31 ± 0.05	16.98 ± 0.05	16.72 ± 0.05	16.36 ± 0.09	15.86 ± 0.09	15.24 ± 0.16
PKS 1450-338	22.52 ± 0.37	20.40 ± 0.10	19.39 ± 0.07	18.69 ± 0.08	16.99 ± 0.08	16.03 ± 0.07	15.23 ± 0.09
PKS 1454-060	18.36 ± 0.06	17.84 ± 0.05	17.45 ± 0.05	17.08 ± 0.05	16.56 ± 0.10	15.86 ± 0.09	15.16 ± 0.15
PKS 1456+044	18.83 ± 0.05	18.12 ± 0.05	16.17 ± 0.05	15.71 ± 0.05	14.30 ± 0.05
PKS 1504-166	20.28 ± 0.12	19.75 ± 0.11	19.35 ± 0.09	18.46 ± 0.10	16.33 ± 0.08	15.59 ± 0.07	14.01 ± 0.07
PKS 1508-055	17.37 ± 0.05	16.94 ± 0.05	16.66 ± 0.05	16.28 ± 0.05	15.56 ± 0.06	14.87 ± 0.06	14.29 ± 0.08
PKS 1509+022	19.75 ± 0.12	18.27 ± 0.06	16.04 ± 0.07	15.12 ± 0.06	14.31 ± 0.08
PKS 1510-089	17.26 ± 0.05	17.12 ± 0.05	16.72 ± 0.05	16.17 ± 0.05	15.24 ± 0.05	14.09 ± 0.05	13.27 ± 0.05
PKS 1511-100	18.18 ± 0.05	18.00 ± 0.05	17.50 ± 0.05	17.07 ± 0.05	16.46 ± 0.07	15.60 ± 0.06	14.70 ± 0.08
PKS 1511-210	22.01 ± 0.25	21.45 ± 0.19	20.65 ± 0.11	20.30 ± 0.16	18.62 ± 0.32	17.81 ± 0.25	16.79 ± 0.36
PKS 1514-241	15.18 ± 0.05	14.50 ± 0.05	13.98 ± 0.05	13.31 ± 0.05	11.95 ± 0.05	11.10 ± 0.05	10.50 ± 0.05
PKS 1518+045	16.11 ± 0.05	14.84 ± 0.05	14.20 ± 0.05	13.45 ± 0.05	12.06 ± 0.05	11.31 ± 0.05	11.02 ± 0.05
PKS 1519-273	18.21 ± 0.06	17.74 ± 0.05	17.18 ± 0.05	16.55 ± 0.05	15.65 ± 0.06	14.84 ± 0.06	14.08 ± 0.07
PKS 1532+016	19.12 ± 0.08	18.92 ± 0.07	18.44 ± 0.06	17.98 ± 0.08	17.40 ± 0.18	16.22 ± 0.11	15.48 ± 0.19
PKS 1535+004	> 21.70	> 22.30	> 21.50	...	> 19.73
PKS 1542+042	18.75 ± 0.06	18.54 ± 0.06	18.21 ± 0.06	17.61 ± 0.06	17.38 ± 0.12	16.46 ± 0.09	15.82 ± 0.17
PKS 1546+027	17.43 ± 0.05	17.14 ± 0.05	16.75 ± 0.05	16.16 ± 0.05	14.97 ± 0.05	13.88 ± 0.05	13.02 ± 0.05
PKS 1548+056	19.37 ± 0.06	18.65 ± 0.06	18.13 ± 0.06	17.42 ± 0.06	16.30 ± 0.07	15.13 ± 0.06	14.30 ± 0.07
PKS 1550-269	20.24 ± 0.14	19.67 ± 0.09	19.18 ± 0.08	18.58 ± 0.10	17.63 ± 0.15	17.01 ± 0.13	16.07 ± 0.11
PKS 1555-140	18.28 ± 0.05	16.93 ± 0.05	16.28 ± 0.05	15.47 ± 0.05	14.25 ± 0.05	13.43 ± 0.05	13.08 ± 0.05
PKS 1555+001	20.34 ± 0.10	19.95 ± 0.08	20.00 ± 0.07	18.72 ± 0.08	17.73 ± 0.16	16.90 ± 0.12	16.24 ± 0.24
PKS 1556-245	18.89 ± 0.06	19.02 ± 0.06	18.82 ± 0.07	18.30 ± 0.08	17.59 ± 0.14	16.97 ± 0.13	16.58 ± 0.31
PKS 1601-222	> 22.90	> 22.40	...	> 20.02	> 19.49
PKS 1602-001	17.66 ± 0.05	17.57 ± 0.05	17.10 ± 0.05	16.66 ± 0.05	16.28 ± 0.07	15.41 ± 0.06	15.19 ± 0.08
PKS 1614+051	20.38 ± 0.11	19.38 ± 0.07	19.31 ± 0.08	18.93 ± 0.10	18.04 ± 0.24	17.83 ± 0.30	17.31 ± 0.32
PKS 1615+029	18.01 ± 0.05	17.75 ± 0.05	17.31 ± 0.05	17.00 ± 0.05	16.66 ± 0.05	16.04 ± 0.05	15.89 ± 0.08
PKS 1616+063	19.45 ± 0.08	18.97 ± 0.06	18.76 ± 0.06	18.27 ± 0.08	17.87 ± 0.21	17.54 ± 0.24	16.52 ± 0.17
PKS 1635-035	21.58 ± 0.32	21.00 ± 0.20	20.75 ± 0.18	20.73 ± 0.33	19.11 ± 0.18	18.84 ± 0.22	17.48 ± 0.32
PKS 1648+015	21.87 ± 0.31	21.14 ± 0.18	20.41 ± 0.11	19.50 ± 0.10	17.84 ± 0.08	16.85 ± 0.06	16.56 ± 0.13
PKS 1649-062	> 23.20	> 23.30	> 18.88	> 17.77	> 17.03
PKS 1654-020	23.51 ± 0.68	23.90 ± 0.87	23.05 ± 0.52	23.02 ± 0.88	> 20.00	19.92 ± 0.64	18.25 ± 0.56
PKS 1655+077	20.18 ± 0.09	19.88 ± 0.07	19.36 ± 0.07	18.42 ± 0.07			

TABLE 4—Continued

Name	B	V	R	I	J	H	K _n
PKS 1958–179	19.48 ± 0.08	18.89 ± 0.06	18.34 ± 0.06	17.54 ± 0.06	16.26 ± 0.08	14.97 ± 0.06	14.39 ± 0.08
PKS 2000–330	18.90 ± 0.06	17.48 ± 0.05	16.92 ± 0.05	16.71 ± 0.05	16.10 ± 0.06	15.64 ± 0.06	15.10 ± 0.08
PKS 2002–185	19.39 ± 0.07	18.82 ± 0.06	18.55 ± 0.06	18.05 ± 0.07	17.03 ± 0.10	16.87 ± 0.10	16.92 ± 0.33
PKS 2004–447	19.52 ± 0.09	18.74 ± 0.06	18.18 ± 0.06	17.35 ± 0.06	16.48 ± 0.07	15.46 ± 0.06	14.70 ± 0.07
PKS 2008–159	17.50 ± 0.05	17.07 ± 0.05	16.76 ± 0.05	16.33 ± 0.05	16.18 ± 0.08	15.58 ± 0.07	14.97 ± 0.12
PKS 2021–330	19.50 ± 0.08	19.06 ± 0.07	18.70 ± 0.06	18.31 ± 0.08	17.70 ± 0.12	16.82 ± 0.09	16.49 ± 0.18
PKS 2022–077	19.10 ± 0.06	18.55 ± 0.05	18.44 ± 0.05	18.50 ± 0.08	18.11 ± 0.30	16.61 ± 0.14	16.08 ± 0.30
PKS 2037–253	19.69 ± 0.09	19.56 ± 0.09	19.21 ± 0.08	19.24 ± 0.16	18.52 ± 0.34	18.01 ± 0.34	17.40 ± 0.66
PKS 2044–168	17.70 ± 0.05	17.55 ± 0.05	17.18 ± 0.05	17.05 ± 0.05	16.48 ± 0.09	15.99 ± 0.09	15.18 ± 0.15
PKS 2047+098	> 22.99	> 22.19	...	> 19.92	...
PKS 2053–044	18.86 ± 0.06	18.47 ± 0.06	18.18 ± 0.06	17.99 ± 0.07	17.81 ± 0.20	16.96 ± 0.15	16.13 ± 0.25
PKS 2056–369	> 23.50	23.45 ± 0.61	22.22 ± 0.44	19.55 ± 0.39	19.07 ± 0.39	18.21 ± 0.41	...
PKS 2058–135	15.88 ± 0.05	14.76 ± 0.05	14.15 ± 0.05	13.45 ± 0.05	12.35 ± 0.05	11.58 ± 0.05	11.39 ± 0.05
PKS 2058–297	18.85 ± 0.06	18.68 ± 0.06	18.29 ± 0.06	18.09 ± 0.07	17.52 ± 0.15	17.00 ± 0.15	16.22 ± 0.35
PKS 2059+034	18.09 ± 0.05	17.65 ± 0.05	17.40 ± 0.05	17.20 ± 0.06	16.34 ± 0.07	16.18 ± 0.08	15.63 ± 0.15
PKS 2106–413	19.57 ± 0.09	18.85 ± 0.06	18.45 ± 0.06	17.76 ± 0.06	16.77 ± 0.08	15.74 ± 0.06	14.81 ± 0.08
PKS 2120+099	19.65 ± 0.10	19.24 ± 0.08	18.96 ± 0.08	18.36 ± 0.10	17.98 ± 0.23	17.66 ± 0.26	16.52 ± 0.34
PKS 2121+053	19.86 ± 0.10	19.22 ± 0.07	18.68 ± 0.06	17.93 ± 0.07	16.52 ± 0.07	15.49 ± 0.06	14.71 ± 0.08
PKS 2126–158	17.97 ± 0.05	16.92 ± 0.05	16.63 ± 0.05	16.23 ± 0.05	15.45 ± 0.05	14.89 ± 0.05	14.30 ± 0.05
PKS 2127–096	19.43 ± 0.07	18.65 ± 0.06	18.00 ± 0.06	17.39 ± 0.06	16.38 ± 0.07	15.41 ± 0.06	14.61 ± 0.08
PKS 2128–123	15.28 ± 0.05	15.13 ± 0.05	15.00 ± 0.05	14.70 ± 0.05	14.58 ± 0.05	13.89 ± 0.05	13.22 ± 0.05
PKS 2131–021	20.61 ± 0.13	20.16 ± 0.15	19.58 ± 0.11	19.11 ± 0.17	17.58 ± 0.14	16.71 ± 0.11	15.85 ± 0.17
PKS 2134+004	17.04 ± 0.05	16.80 ± 0.05	16.56 ± 0.05	16.11 ± 0.05	15.67 ± 0.06	15.18 ± 0.06	14.73 ± 0.08
PKS 2135–248	19.64 ± 0.10	19.23 ± 0.08	18.96 ± 0.08	18.41 ± 0.10	17.50 ± 0.13	16.76 ± 0.11	15.89 ± 0.18
PKS 2140–048	17.22 ± 0.05	17.18 ± 0.05	16.87 ± 0.05	16.44 ± 0.05	15.59 ± 0.05	14.76 ± 0.05	13.95 ± 0.06
PKS 2143–156	18.02 ± 0.05	17.69 ± 0.05	17.55 ± 0.05	17.09 ± 0.06	16.61 ± 0.08	15.91 ± 0.07	15.24 ± 0.11
PKS 2144+092	18.78 ± 0.07	18.36 ± 0.06	18.01 ± 0.06	17.68 ± 0.07	16.37 ± 0.07	15.69 ± 0.07	14.82 ± 0.09
PKS 2145–176	19.43 ± 0.09	19.11 ± 0.08	18.85 ± 0.07	18.23 ± 0.09	17.74 ± 0.19	17.25 ± 0.19	16.41 ± 0.32
PKS 2145+067	16.15 ± 0.05	15.80 ± 0.05	15.56 ± 0.05	15.29 ± 0.05	14.54 ± 0.05	14.17 ± 0.05	13.48 ± 0.06
PKS 2149–307	18.00 ± 0.05	17.75 ± 0.05	17.31 ± 0.05	17.20 ± 0.06	16.60 ± 0.08	16.02 ± 0.08	15.24 ± 0.13
PKS 2149+056	> 23.50	22.05 ± 0.23	20.85 ± 0.11	19.54 ± 0.10	18.26 ± 0.24	17.42 ± 0.18	17.17 ± 0.49
PKS 2149+069	18.79 ± 0.07	18.48 ± 0.06	17.99 ± 0.06	17.74 ± 0.06	16.90 ± 0.10	15.82 ± 0.07	15.76 ± 0.19
PKS 2155–152	18.42 ± 0.05	17.90 ± 0.05	17.45 ± 0.05	16.88 ± 0.05	15.67 ± 0.05	14.72 ± 0.05	13.92 ± 0.05
PKS 2200–238	18.45 ± 0.06	18.36 ± 0.06	18.10 ± 0.06	17.64 ± 0.07	17.27 ± 0.11	16.72 ± 0.11	15.82 ± 0.09
PKS 2203–188	18.85 ± 0.07	18.52 ± 0.06	18.10 ± 0.06	17.46 ± 0.06	16.69 ± 0.08	15.93 ± 0.07	15.25 ± 0.07
PKS 2206–237	17.41 ± 0.06	16.25 ± 0.05	15.70 ± 0.05	15.04 ± 0.05	13.94 ± 0.05	13.23 ± 0.05	12.87 ± 0.06
PKS 2208–137	16.79 ± 0.05	16.70 ± 0.05	16.42 ± 0.05	16.10 ± 0.05	15.13 ± 0.05	14.34 ± 0.05	13.40 ± 0.05
PKS 2210–257	18.74 ± 0.07	18.76 ± 0.07	18.53 ± 0.06	17.95 ± 0.07	17.34 ± 0.12	16.42 ± 0.09	15.65 ± 0.08
PKS 2212–299	17.47 ± 0.05	17.36 ± 0.05	17.12 ± 0.05	16.81 ± 0.05	15.92 ± 0.06	15.19 ± 0.06	14.59 ± 0.06
PKS 2215+020	21.84 ± 0.31	20.42 ± 0.10	20.14 ± 0.12	20.00 ± 0.20	19.20 ± 0.50	18.21 ± 0.29	19.34 ± 1.78
PKS 2216–038	17.03 ± 0.05	16.49 ± 0.05	16.14 ± 0.05	15.80 ± 0.05	14.81 ± 0.05	14.42 ± 0.05	13.96 ± 0.05
PKS 2223–052	18.59 ± 0.06	18.33 ± 0.06	17.89 ± 0.05	17.43 ± 0.06	16.45 ± 0.07	15.51 ± 0.06	14.69 ± 0.06
PKS 2227–088	18.31 ± 0.06	18.15 ± 0.06	17.81 ± 0.05	17.39 ± 0.06	16.47 ± 0.07	15.70 ± 0.06	15.06 ± 0.09
PKS 2227–399	17.94 ± 0.05	17.77 ± 0.05	17.19 ± 0.05	16.69 ± 0.05	15.87 ± 0.06	15.02 ± 0.05	14.11 ± 0.06
PKS 2229–172	21.26 ± 0.19	21.14 ± 0.18	21.34 ± 0.30	19.83 ± 0.17	18.88 ± 0.27	17.71 ± 0.21	16.77 ± 0.17
PKS 2233–148	19.24 ± 0.06	18.61 ± 0.06	18.06 ± 0.05	17.27 ± 0.05	16.38 ± 0.06	15.42 ± 0.06	14.57 ± 0.05
PKS 2239+096	19.00 ± 0.06	18.68 ± 0.06	18.34 ± 0.06	17.91 ± 0.06	17.42 ± 0.12	16.73 ± 0.10	16.01 ± 0.18
PKS 2240–260	17.95 ± 0.05	17.37 ± 0.05	16.95 ± 0.05	16.36 ± 0.05	15.15 ± 0.05	14.32 ± 0.05	13.52 ± 0.05
PKS 2243–123	16.65 ± 0.05	16.50 ± 0.05	16.32 ± 0.05	16.04 ± 0.05	15.51 ± 0.05	15.00 ± 0.05	14.50 ± 0.07
PKS 2245–328	19.08 ± 0.07	18.82 ± 0.07	18.51 ± 0.06	18.31 ± 0.08	17.61 ± 0.13	17.20 ± 0.14	16.08 ± 0.19
PKS 2245+029	21.71 ± 0.22	21.00 ± 0.17	20.26 ± 0.10	19.48 ± 0.11	17.45 ± 0.14	16.63 ± 0.12	15.49 ± 0.15
PKS 2252–090	22.03 ± 0.24	21.51 ± 0.16	20.49 ± 0.12	19.48 ± 0.11	18.98 ± 0.49	17.02 ± 0.16	16.48 ± 0.33
PKS 2312–319	18.10 ± 0.05	17.86 ± 0.05	17.50 ± 0.05	17.09 ± 0.05	16.82 ± 0.09	16.04 ± 0.08	15.63 ± 0.09
PKS 2313–438	18.89 ± 0.11	19.53 ± 0.08	19.10 ± 0.07	18.63 ± 0.10	17.97 ± 0.19	17.37 ± 0.18	16.72 ± 0.17
PKS 2314–409	18.33 ± 0.06	18.08 ± 0.05	17.75 ± 0.05	17.36 ± 0.06	16.74 ± 0.08	16.15 ± 0.08	15.59 ± 0.08
PKS 2329–415	19.40 ± 0.08	19.17 ± 0.07	18.89 ± 0.07	18.41 ± 0.09	17.58 ± 0.14	16.67 ± 0.10	15.67 ± 0.08
PKS 2337–334	22.93 ± 0.60	21.89 ± 0.27	21.40 ± 0.20	20.51 ± 0.14	19.88 ± 0.54	18.42 ± 0.32	16.39 ± 0.20
PKS 2344–192	23.52 ± 0.68	...	21.68 ± 0.25	20.96 ± 0.27	18.71 ± 0.13	17.64 ± 0.09	17.25 ± 0.20
PKS 2345–167	17.23 ± 0.05	16.79 ± 0.05	16.44 ± 0.05	15.88 ± 0.05	14.53 ± 0.05	13.57 ± 0.05	12.76 ± 0.05
PKS 2351–154	18.97 ± 0.07	18.71 ± 0.06	18.46 ± 0.06	18.42 ± 0.10	17.88 ± 0.18	17.06 ± 0.14	16.37 ± 0.26
PKS 2354–117	18.81 ± 0.07	18.03 ± 0.05	17.80 ± 0.05	17.44 ± 0.06	16.56 ± 0.07	15.96 ± 0.07	15.06 ± 0.06
L 2110–4509	18.89 ± 0.07	18.64 ± 0.07	18.21 ± 0.06	17.78 ± 0.08	16.19 ± 0.06	15.37 ± 0.06	15.13 ± 0.10
L 2111–4335	17.29 ± 0.05	16.78 ± 0.05	16.54 ± 0.05	15.99 ± 0.05	15.25 ± 0.05	14.55 ± 0.05	14.33 ± 0.07
L 2111–4506	17.54 ± 0.05	17.37 ± 0.05	16.94 ± 0.05	16.73 ± 0.05	16.16 ± 0.06	15.35 ± 0.06	15.32 ± 0.12
L 2113–4305	17.87 ± 0.05	17.62 ± 0.05	17.18 ± 0.05	16.92 ± 0.06	16.39 ± 0.07	15.96 ± 0.07	15.21 ± 0.11
L 2113–4345	18.56 ± 0.06	18.22 ± 0.06	17.99 ± 0.06	17.62 ± 0.07	17.12 ± 0.10	16.86 ± 0.12	16.21 ± 0.23
L 2113–4538	17.67 ± 0.05	17.49 ± 0.05	17.27 ± 0.05	16.89 ± 0.06
L 2114–4335	18.22 ± 0.06	17.90 ± 0.05	17.52 ± 0.05	17.25 ± 0.05
L 2114–4346	18.56 ± 0.06	18.42 ± 0.06	18.09 ± 0.06	17.79 ± 0.06
L 2114–4501	18.67 ± 0.06	18.54 ± 0.06	18.49 ± 0.06	18.05 ± 0.07
L 2116–4439	18.61 ± 0.06	18.20 ± 0.06	17.80 ± 0.05	17.40 ± 0.06
L 2118–4702	19.21 ± 0.08	18.98 ± 0.07	18.64 ± 0.06	18.40 ± 0.08	16.67 ± 0.30
L 2119–4415	18.02 ± 0.05	17.72 ± 0.05	17.43 ± 0.05	16.88 ± 0.05	16.07 ± 0.06	15.68 ± 0.06	15.03 ± 0.09